

## CANCER

# The spindle assembly checkpoint is a therapeutic vulnerability of CDK4/6 inhibitor-resistant ER<sup>+</sup> breast cancer with mitotic aberrations

Isabel Soria-Bretones<sup>1,2,3†</sup>, Kelsie L. Thu<sup>1,4,5</sup>, Jennifer Silvester<sup>1</sup>, Jennifer Cruickshank<sup>1</sup>, Samah El Ghamrasni<sup>1</sup>, Wail Ba-alawi<sup>1</sup>, Graham C. Fletcher<sup>1‡</sup>, Reza Kiarash<sup>1‡</sup>, Mitchell J. Elliott<sup>1,6</sup>, Jordan J. Chalmers<sup>1</sup>, Andrea C. Elia<sup>1</sup>, Albert Cheng<sup>1</sup>, April A. N. Rose<sup>2,3</sup>, Mark R. Bray<sup>1‡</sup>, Benjamin Haibe-Kains<sup>1</sup>, Tak W. Mak<sup>1</sup>, David W. Cescon<sup>1,6\*</sup>

Copyright © 2022  
The Authors, some  
rights reserved;  
exclusive licensee  
American Association  
for the Advancement  
of Science. No claim to  
original U.S. Government  
Works. Distributed  
under a Creative  
Commons Attribution  
NonCommercial  
License 4.0 (CC BY-NC).

Inhibitors of cyclin-dependent kinases 4 and 6 (CDK4/6i) are standard first-line treatments for metastatic ER<sup>+</sup> breast cancer. However, acquired resistance to CDK4/6i invariably develops, and the molecular phenotypes and exploitable vulnerabilities associated with resistance are not yet fully characterized. We developed a panel of CDK4/6i-resistant breast cancer cell lines and patient-derived organoids and demonstrate that a subset of resistant models accumulates mitotic segregation errors and micronuclei, displaying increased sensitivity to inhibitors of mitotic checkpoint regulators TTK and Aurora kinase A/B. *RB1* loss, a well-recognized mechanism of CDK4/6i resistance, causes such mitotic defects and confers enhanced sensitivity to TTK inhibition. In these models, inhibition of TTK with CFI-402257 induces premature chromosome segregation, leading to excessive mitotic segregation errors, DNA damage, and cell death. These findings nominate the TTK inhibitor CFI-402257 as a therapeutic strategy for a defined subset of ER<sup>+</sup> breast cancer patients who develop resistance to CDK4/6i.

## INTRODUCTION

Estrogen receptor (ER)-positive, human epidermal growth factor receptor 2 (HER2)-negative (ER<sup>+</sup>/HER2<sup>-</sup>) is the most common subtype of breast cancer, accounting for up to 70% of all cases diagnosed. Most patients with early ER<sup>+</sup>/HER2<sup>-</sup> breast cancer have good outcomes following treatment with local (surgery and/or radiation) and (neo)adjuvant systemic endocrine therapies (i.e., selective estrogen receptor modulators and aromatase inhibitors), as well as chemotherapy for selected patients. However, relapses of ER<sup>+</sup>/HER2<sup>-</sup> breast cancer remain a major problem, comprising 60% of metastatic breast cancer (1). While median survival has improved, metastatic ER<sup>+</sup>/HER2<sup>-</sup> disease is generally incurable (2).

In ER<sup>+</sup> breast cancer, estrogen drives cell proliferation by inducing the expression of cyclin D1 and activating the cyclin-dependent kinase 4/6 (CDK4/6) pathway (3, 4). In a complex with cyclin D, CDK4/6 phosphorylates the retinoblastoma protein (Rb), leading to release of the transcription factor E2F, which drives the expression of downstream cell cycle genes and promotes cell cycle progression through the G<sub>1</sub>-S checkpoint. This biology underlies the therapeutic effects of CDK4/6 inhibitors (CDK4/6i) (palbociclib, ribociclib, and abemaciclib), which were identified as clinically effective drugs for ER<sup>+</sup> disease and have been rapidly adopted as standard of care therapies for metastatic ER<sup>+</sup>/HER2<sup>-</sup> breast cancer in combination with endocrine therapy (5). Despite demonstrating improvements

in overall and disease-free survival, resistance to combined CDK4/6i and endocrine therapy invariably develops (6–12). Thus, there is an urgent clinical need to understand CDK4/6i-resistant disease, its genomic and molecular features, as well as its vulnerabilities to identify and develop effective therapeutic strategies for these patients.

To date, numerous genomic alterations affecting cell cycle-related genes have been demonstrated to induce acquired resistance to CDK4/6i in patients and preclinical models. These alterations include loss of *RB1* and *FAT1*; down-regulation of the intrinsic CDK4/6 repressors p27 and p21; activating mutations in the phosphatidylinositol 3-kinase (PI3K) signaling pathway; amplification of *CDK6*, *CCNE1*, *FGFR1*, and *AURKA*; and up-regulation of cyclin D1, cyclin D2, CDK2, MYC, PDK1, and SKP2, among others (4, 13–19). The diversity of mechanisms that have been associated with CDK4/6i resistance has complicated the understanding of this disease entity, as well as the development of second-line therapeutic strategies to effectively address it. However, most of the genomic alterations described in CDK4/6i-resistant tumors thus far converge on their capacity to directly or indirectly override the G<sub>1</sub>-S checkpoint imposed by Rb. The G<sub>1</sub>-S cell cycle checkpoint contributes to the maintenance of genome integrity by avoiding DNA replication in suboptimal conditions (i.e., damaged DNA or insufficient cell size, low nutrient, growth factors, and nucleotide levels) and ensuring expression of genes that are necessary for downstream cell cycle progression. Therefore, weakened or nonfunctional G<sub>1</sub>-S checkpoint signaling leads to replication stress and the accumulation of DNA damage, genomic instability, and aberrant chromosome segregation (20–23). Consistent with CDK4/6i-resistant cells being able to escape G<sub>1</sub>-S checkpoint, analyses of clinical samples have identified increases in markers of genomic instability following progression on palbociclib treatment (24, 25). Mounting evidence suggests that the genomic instability and mitotic errors caused by G<sub>1</sub>-S checkpoint dysfunction represent a therapeutic vulnerability that can be exploited for the treatment of cancer by further deregulating cancer cell mitosis

<sup>1</sup>Princess Margaret Cancer Centre, University Health Network, Toronto, ON, Canada.

<sup>2</sup>Segal Cancer Centre and Lady Davis Institute for Medical Research, Jewish General Hospital, Montreal, QC, Canada. <sup>3</sup>Gerald Bronfman Department of Oncology, McGill University, Montreal, QC, Canada. <sup>4</sup>Keenan Research Centre for Biomedical Sciences, St. Michael's Hospital, Toronto, ON, Canada. <sup>5</sup>Laboratory Medicine and Pathobiology, University of Toronto, Toronto, ON, Canada. <sup>6</sup>Department of Medicine, University of Toronto, Toronto, ON, Canada.

\*Corresponding author. Email: dave.cescon@uhn.ca

†Present address: Repare Therapeutics, Montreal, QC, Canada.

‡Present address: Treadwell Therapeutics, Toronto, ON, Canada.

with targeted inhibitors. For instance, *RBI* loss, which causes chromosome segregation errors, micronuclei, and DNA damage in different tumor models, induces sensitivity to targeted inhibitors of the mitotic regulators polo-like kinase 1 (PLK1) and Aurora kinase A/B (20, 22, 26–29). Moreover, Gallo *et al.* (30) have demonstrated that *CCNE1* overexpression, which can override the G<sub>1</sub>-S checkpoint and cause resistance to CDK4/6i, sensitizes cancer cells to PKMYT1 inhibition, causing cell death through premature entry into mitosis and mitotic catastrophe. A recent study by Crozier *et al.* (31) demonstrated that short-term CDK4/6i treatment induced replication stress and genomic instability in immortalized RPE1 cells. Given the specific importance of CDK4/6i in ER<sup>+</sup> breast cancer, we investigated the impact of long-term CDK4/6i treatment on the induction of genomic instability and mitotic errors in preclinical breast cancer models and evaluated the activity of novel and clinically relevant mitotic kinase inhibitors for the treatment of CDK4/6i-resistant ER<sup>+</sup> breast cancer.

## RESULTS

### A subset of palbociclib-resistant models displays increased mitotic defects associated with genomic instability

To investigate genomic instability and mitotic defects caused by CDK4/6i resistance in different genomic backgrounds, we generated models of acquired resistance to palbociclib (Palbo-R) via sequential dose escalation in a panel of eight ER<sup>+</sup> breast cancer cell lines and an ER<sup>+</sup>, CDK4/6i-sensitive, patient-derived breast cancer organoid model (PDO; designated BPTO.95) (Fig. 1A; fig. S1, A and B; and table S1). After dose escalation, palbociclib was withdrawn from Palbo-R culture medium to avoid the confounding effects of ongoing treatment on subsequent experiments. The degree of resistance was variable across the panel of Palbo-R models, with some achieving strong insensitivity to palbociclib [median inhibitory concentration (IC<sub>50</sub>) > 1 μM; T47D, LY2, HCC1428, and BPTO.95], while others retained partial sensitivity (Fig. 1, B and C, and fig. S2, A and B). Cross-resistance to the CDK4/6i abemaciclib was observed in most of the models (fig. S2, C and D). Consistent with the variety of mechanisms that can lead to CDK4/6i resistance and the variability in the degree of resistance we observed in our panel, analysis of specific cell cycle-related genes revealed heterogeneous expression profiles and genomic alterations across the Palbo-R models (fig. S2, E to H, and tables S2 and S3). We found diverse alterations in genes that have been reported in preclinical and clinical studies of CDK4/6i resistance, including *RBI* [copy number (CN) loss in T47D, LY2, and ZR-75-1; splice mutations in LY2 and ZR-75-1; decreased gene expression in MDA-MB-361 and ZR-75-1; and complete loss of *Rb* gene and protein expression in LY2], *FAT1* (shallow deletion in MDA-MB-361; decreased gene expression in MDA-MB-361, KPL-1, and ZR-75-1; and profound decreased expression in MCF7 and BPTO.95), *CDK6* (shallow amplification in CAMA-1 and HCC1428; over 10-fold increased gene expression in HCC1428), *CCND1* (shallow amplification and increased gene expression in MCF7), *CCNE1* (shallow amplifications in T47D and KPL-1; amplification in MCF7; increased gene expression in T47D), *CCNE2* (shallow amplification in MCF7, over 2-fold increased gene expression in MCF7 and CAMA-1), *CDKN1A* (decreased gene expression below 0.5-fold in T47D, MDA-MB-361, and ZR-75-1), *FGFR2* (over 2-fold increased gene expression in T47D and BPTO.95 #1), *KRAS* (amplification in T47D), *PDK1* (increased gene expression in MCF7), and *TK1* (amplification in MCF7).

To investigate whether Palbo-R models accumulate genomic instability as a consequence of escaping long-term CDK4/6i inhibition, we first analyzed the incidence of micronuclei, which are well-established markers of chromosome missegregation leading to genomic instability (32). Three of the Palbo-R cell lines (T47D, MDA-MB-361, and LY2) exhibited notable increases in micronuclei abundance compared to their parental lines (Fig. 1D and fig. S3A), suggesting that a subset of CDK4/6i resistance mechanisms are associated with genomic instability. Next, we hypothesized that the increased incidence of micronuclei observed could be the result of an increase in mitotic segregation errors. To analyze this, we performed live-cell microscopy and assessed mitotic phenotypes in dividing cells (fig. S3B). Supporting our hypothesis, Palbo-R cells with increased micronuclei displayed a higher frequency of abnormal mitoses, including mild segregation errors (i.e., micronuclei, anaphase bridges, and lagging chromosomes), severe segregation errors (i.e., multiple micronuclei, thick anaphase bridges, asymmetric segregation, multipolar spindles, and multinucleated cells), and mitotic exit without segregation (Fig. 1E). Palbo-R BPTO.95 PDO also displayed increased mitotic errors, with a clear increase in mitoses with multipolar spindles (Fig. 1, E and F). Along with increased mitotic errors, these Palbo-R models also spent more time in mitosis, suggesting an activation of the mitotic checkpoint in response to defects in mitotic progression (Fig. 1G). The DNA damage marker H2AX pSer<sup>139</sup> (γH2AX) was elevated in most of the Palbo-R models relative to parental controls, including some with low incidences of micronuclei (fig. S3C), revealing an accumulation of endogenous DNA damage that appears distinct from chromosome segregation errors.

Together, these results show that ER<sup>+</sup> breast cancer cells can accumulate hallmarks of genomic instability upon development of CDK4/6i resistance. We define a subset of CDK4/6i-resistant models with increased mitotic defects and micronuclei formation.

### CDK4/6i-resistant models with increased mitotic aberrations are hypersensitive to TTK and Aurora kinase inhibitors

We next hypothesized that the subset of Palbo-R models with increased mitotic defects, such as increased incidence of micronuclei and segregation errors, might be sensitive to mitotic kinase inhibitors that potentiate genomic instability to induce lethality. To test this hypothesis, we performed drug dose-response assays in the matched Palbo-R and parental ER<sup>+</sup> breast cancer cell lines using targeted inhibitors of different mitotic kinases. Our group has recently developed and characterized a potent and selective inhibitor of the spindle assembly checkpoint (SAC) kinase TTK, CFI-402257, which induces premature chromosome segregation and has demonstrated strong antitumor activity in triple-negative breast cancer cell lines (33). Therefore, we aimed to assess the sensitivity of Palbo-R cells to CFI-402257, as well as to additional inhibitors targeting other relevant mitotic kinases, i.e., Aurora kinase B (barasertib), Aurora kinase A (alisertib), PLK1 (volasertib), CDK1 (RO-3306), and a pan-Aurora kinase inhibitor (tozasertib) (fig. S4A). Evaluation of area above the curve (AAC) and growth inhibition values for each drug showed that Palbo-R cell lines with increased micronuclei were hypersensitive to CFI-402257 and Aurora kinase A/B inhibition (Fig. 2, A and B) but not to PLK1 or CDK1 inhibition (fig. S4B). Consistent hypersensitivity to additional TTK inhibitors (TTKi) (NMS-P715 and MPI-0479605) was observed (fig. S4C). There was a strong positive correlation between drug sensitivity and micronuclei count for TTK and Aurora kinase inhibitors, when considering all

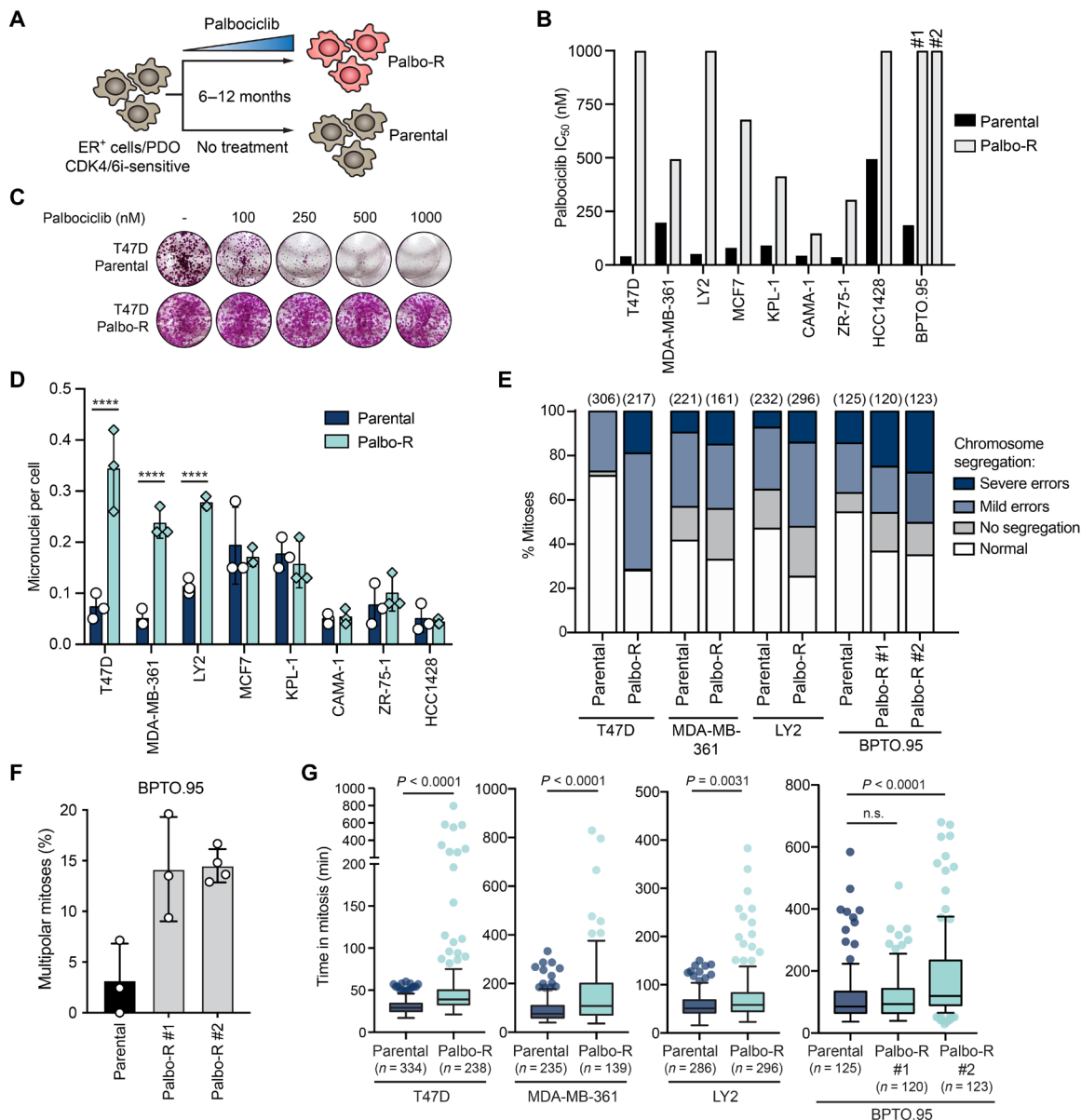


**Fig. 1. A subset of CDK4/6i-resistant models exhibit increased micronuclei and mitotic errors.** (A) Dose-escalation strategy was followed to generate palbociclib resistance in cells and PDOs (BPTO.95). (B) Comparison of absolute  $IC_{50}$  values for palbociclib in Palbo-R and parental cells and BPTO.95 PDO (two resistant lines #1 and #2). A single  $IC_{50}$  value was calculated from the average of three independent experiments. Palbo-R T47D, LY2, ZR-75-1, and BPTO.95 values are capped at the maximum experimental dose of palbociclib. (C) Images of a representative pair of Palbo-R and parental cell lines showing cell survival after 14 days of palbociclib treatment. (D) Micronuclei were counted by immunofluorescence. At least 500 individual cells were counted per experiment. Mean  $\pm$  SD of the relative micronuclei incidence per cell from three independent experiments is plotted.  $P$  values indicate significance for two-way analysis of variance (ANOVA) with uncorrected Fisher's least significant difference test; \*\*\*\* $P < 0.0001$ . (E) Quantification of the mitotic phenotypes observed in Palbo-R and parental models by live-cell imaging. Pooled data from at least two independent experiments are plotted. Numbers in brackets indicate the total number of cells analyzed. (F) Proportion of mitoses with multipolar spindles detected in Palbo-R and parental BPTO.95 PDO by live-cell microscopy. (G) Duration of mitosis was measured from nuclear envelope breakdown until mitotic exit. Pooled data from at least two independent experiments are plotted using the Tukey boxplot method. Numbers in brackets indicate the total number of cells analyzed per cell line.  $P$  values indicate significance for Kolmogorov-Smirnov nonparametric test. n.s., not significant.

parental and Palbo-R cells together (fig. S4D). In addition, Palbo-R PDO models, which have increased mitotic errors, were also hypersensitive to CFI-402257 and Aurora kinase inhibitors (Fig. 2C). To further demonstrate the differential cytotoxic response of Palbo-R cells to these mitotic kinase inhibitors, we analyzed the apoptosis marker annexin V in the most responsive Palbo-R cell line, MDA-MB-361,

after CFI-402257 and barasertib treatments, and observed a significant and dose-dependent increase in apoptosis in the Palbo-R line compared to the parental (Fig. 2D).

Collectively, these results demonstrate that selective inhibitors of the mitotic checkpoint kinases TTK and Aurora A/B have increased antiproliferative and cytotoxic effects in CDK4/6i-resistant

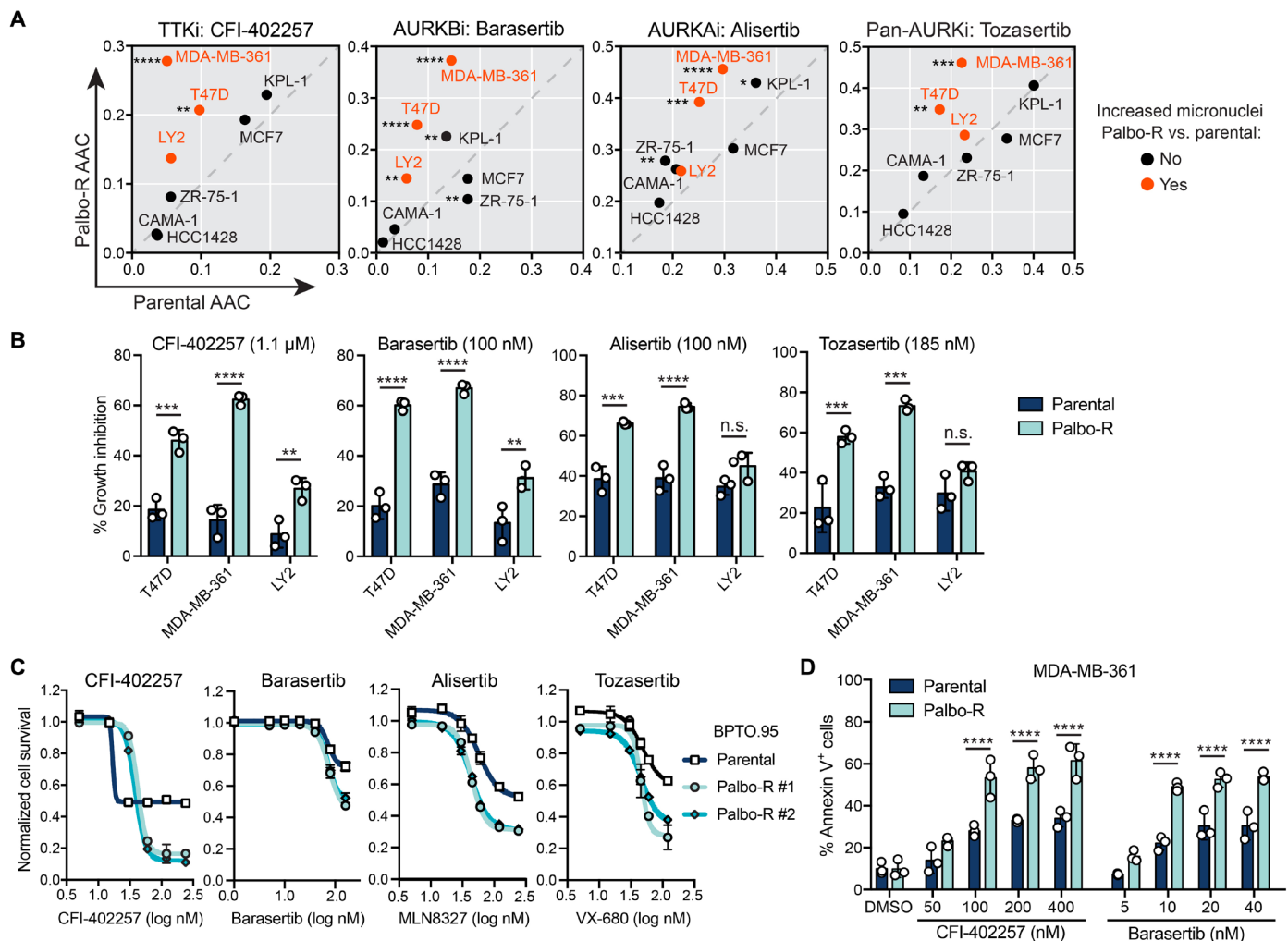


**Fig. 2. Increased sensitivity to TTK and Aurora kinase A/B inhibitors in Palbo-R models with increased micronuclei and mitotic errors.** (A) Comparison of sensitivity to TTK and Aurora kinase A/B inhibitors measured as area above the dose-response curve (AAC) for matched Palbo-R and parental lines. Each dot represents the mean AAC value from three independent dose-response curves for a given pair of cell lines. Dots above the dashed line show higher drug sensitivity (higher AAC) in Palbo-R relative to its matched parental line. Palbo-R cell lines with increased micronuclei incidence are depicted in orange. (B) Growth inhibition caused by TTK and Aurora kinase A/B inhibitors on Palbo-R lines with increased micronuclei and matched parentals. Drug concentrations were selected to reflect the maximum inhibitory effect (i.e., doses at which a plateau was reached in the dose-response assays). Data represent mean  $\pm$  SD of three independent experiments. (C) Dose-response assay for TTK and Aurora kinase A/B inhibitors on BPTO.95 PDO treated for 14 days. Representative experiments out of three independent replicates are shown. Data represent mean  $\pm$  SD of two technical replicates. (D) Apoptosis induced by CFI-402257 and barasertib (5-day treatment) in MDA-MB-361 measured by annexin V staining. Mean  $\pm$  SD of three independent experiments is shown. *P* values indicate significance for two-tailed Student's *t* test (AAC values), two-way ANOVA with Sidak's multiple comparison test (growth inhibition and annexin V). \**P* < 0.05; \*\**P* < 0.01; \*\*\**P* < 0.001; \*\*\*\**P* < 0.0001.

breast cancer models exhibiting higher levels of mitotic errors than in their parental, palbociclib-sensitive counterparts.

**RB1 loss sensitizes ER<sup>+</sup> breast cancer to the TTKi CFI-402257**

Loss of function of Rb is one of the best-characterized clinically observed mechanisms of resistance to CDK4/6i and is known to cause chromosome segregation errors, micronuclei, and DNA damage in different tumor models (20, 26, 29, 34). Furthermore, RB1 loss induces sensitivity to Aurora kinase inhibitors (27, 28). Accordingly, one of our Palbo-R lines, LY2, acquired complete loss of Rb protein expression, increased micronuclei and mitotic errors, and displayed increased sensitivity to Aurora kinase B inhibition (Figs. 1, D and E, and 2, A and B, and fig. S2E). LY2 Palbo-R was also more sensitive

to the TTKi CFI-402257. To experimentally test whether RB1 loss induces sensitivity to TTK inhibition, we inactivated RB1 using the CRISPR-Cas9 system in four ER<sup>+</sup> breast cancer cell lines and the BPTO.95 PDO model (Fig. 3, A to C). As expected, Rb depletion conferred strong resistance to CDK4/6i in these models, confirmed by colony survival assays (fig. S5, A and B). All RB1-deficient (RB1<sup>-/-</sup>) clonal cell lines and the sgRB1-transduced PDO population were consistently more sensitive to CFI-402257 than were their matched parental models (Fig. 3, D and E, and fig. S5C). These effects were not associated with any differences in proliferation (fig. S5, D and E). In the p53 wild-type cell lines MCF7 and KPL-1, CFI-402257 treatment activated the p53 pathway, evidenced by p53 stabilization and accumulation of the downstream cell cycle regulator p21.

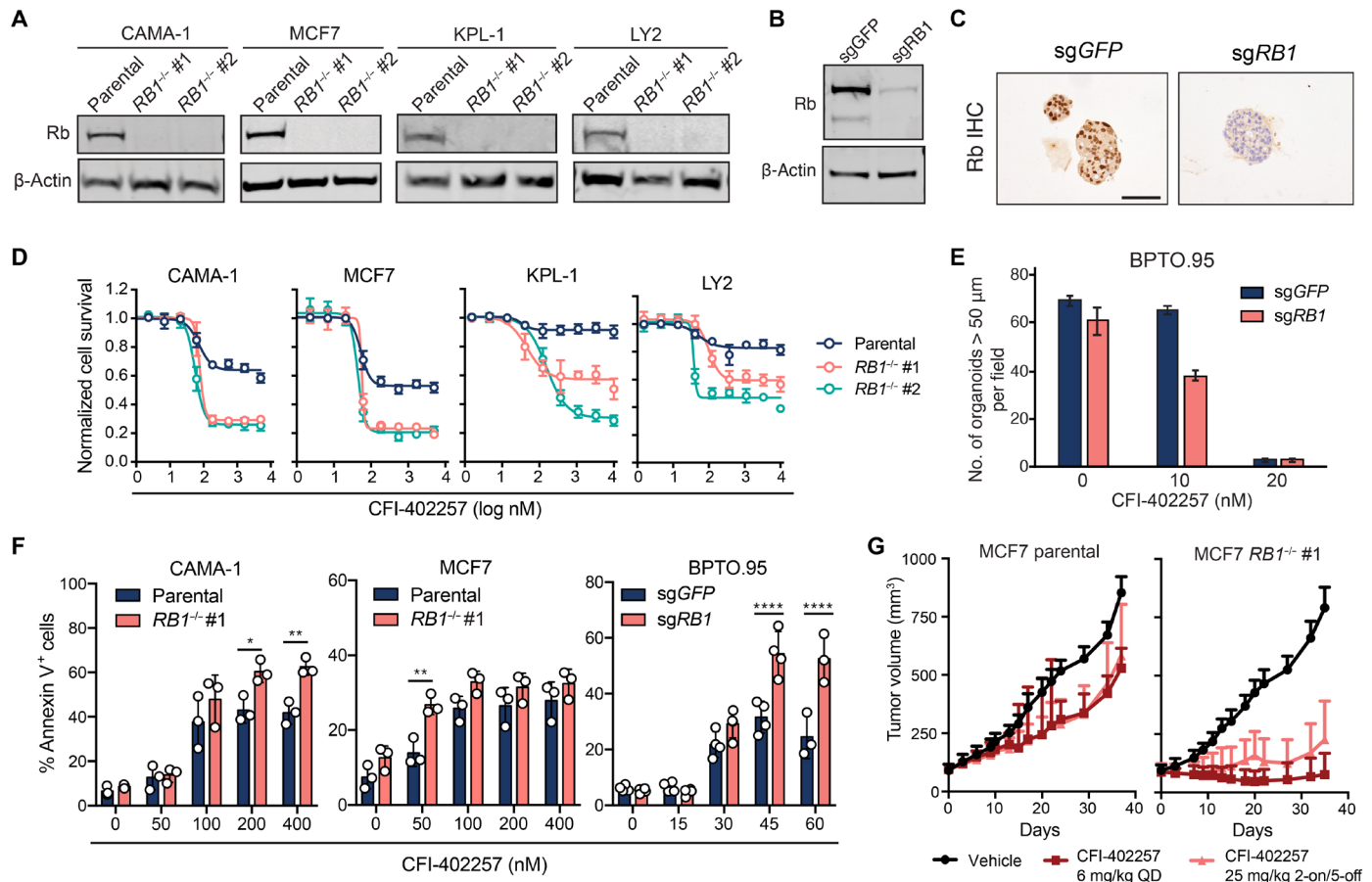


**Fig. 3. RB1 loss is synthetic lethal with TTK inhibition by CFI-402257.** (A) CRISPR-mediated *RB1* knockout (*RB1*<sup>-/-</sup>) in independent clonal cell lines confirmed by immunoblot. (B and C) Decrease in overall Rb expression in a polyclonal ER<sup>+</sup> PDO population achieved through CRISPR-mediated *RB1* editing (*sgRB1*) demonstrated by immunoblot (B) and immunohistochemistry (IHC) (C). Scale bar, 100  $\mu$ m. (D) Response of independent *RB1*<sup>-/-</sup> clones to CFI-402257. Dose-response curves were generated using SRB assays with serial drug dilutions. For each drug dose, cell viability is plotted as the proportion of viability observed in DMSO-treated control cells. Cells were treated for 5 days before fixing and staining with SRB. Mean  $\pm$  SD of six technical replicates of a representative experiment is shown. (E) Quantitation of viable *sgRB1* versus control organoids treated with CFI-402257 for 14 days. (F) Assessment of apoptosis induction by CFI-402257 in *RB1*<sup>-/-</sup> cell lines and *sgRB1* PDO measured by annexin V staining. Mean  $\pm$  SD of three independent experiments is shown. (G) In vivo activity of CFI-402257 on *RB1*<sup>-/-</sup> and wild-type MCF7-derived tumor xenografts. SCID mice with established MCF7 xenografts were treated for up to 38 days ( $n = 6$  mice per arm).  $P$  values indicate significance for two-way ANOVA with Sidak's multiple comparison test (annexin V staining). \* $P < 0.05$ ; \*\* $P < 0.01$ ; \*\*\*\* $P < 0.0001$ .

CFI-402257-induced activation of p53 was more pronounced in *RB1*<sup>-/-</sup> clones than in the matched parental lines (fig. S5, F and G). Levels of the apoptotic marker annexin V levels after CFI-402257 treatment were higher (CAMA-1 and BPTO.95) and achieved at lower doses (MCF7) in *RB1*<sup>-/-</sup> models compared to matched control models (Fig. 3F). Induction of apoptosis in CAMA-1 *RB1*<sup>-/-</sup> was further confirmed by detection of cleaved caspase-3 72 hours after CFI-402257 treatment (fig. S5H). At the doses used in these experiments, CFI-402257 demonstrated dose-dependent reduction of the mitotic marker phospho-histone H3 (Ser<sup>10</sup>), consistent with TTK inhibition even at low doses used in BPTO.95 organoids (fig. S5, I and J) (33, 35).

To determine whether the enhanced in vitro sensitivities observed extend to tumor responses in vivo, we assessed the efficacy of CFI-402257 in xenografts derived from *RB1*-deficient MCF7 cells. CFI-402257 administered orally resulted in partial tumor growth inhibition (TGI) in parental, *RB1*-proficient tumors (6 mg/kg CFI-402257 daily, TGI = 41%; 25 mg/kg CFI-402257 2 days on/5 days

off, TGI = 34%). In contrast, CFI-402257 had profound antitumor activity in *RB1*-deficient xenografts, achieving nearly completed inhibition of tumor growth when dosed on the daily schedule (6 mg/kg CFI-402257 daily, TGI = 90%; 25 mg/kg CFI-402257 2 days on/5 days off, TGI = 70%) (Fig. 3G). Consistent with previous in vivo studies in various tumor models (33), CFI-402257 was well tolerated at the doses used, as demonstrated by mouse weight loss of no more than 10% (fig. S5K).

We next asked whether loss of the Rb checkpoint, a phenomenon that is recurrent in breast cancer, could serve as a biomarker for CFI-402257 sensitivity across breast cancer subtypes, in the absence of any previous CDK4/6i treatment. For this, we applied a pharmacogenomic approach and interrogated a comprehensive collection of 52 cell lines representing the main breast cancer subtypes [ER<sup>+</sup>, ER<sup>-</sup>/HER2<sup>-</sup> (triple-negative), and HER2<sup>+</sup>], in which we had previously characterized CFI-402257 response and which had gene expression profiles available (36). We leveraged independently established gene signatures indicative of Rb-E2F checkpoint deficiency (37–39) and

calculated *RB1*-loss scores for each of the breast cancer cell lines (fig. S5L). All three of the tested signatures showed strong positive correlations with CFI-402257 AAC values, indicating that a weakened Rb checkpoint correlates with higher sensitivity to CFI-402257 in breast cancer cell lines, independently of their molecular subtype. This suggests that the increased sensitivity to CFI-402257 caused by *RB1* deficiency that we observed in ER<sup>+</sup> cell lines can be extended to all breast cancer subtypes, including those with a weakened Rb checkpoint, and independent of prior CDK4/6i treatment.

Together, these results indicate that the TTKi CFI-402257 is synthetic lethal with *RB1* loss and can efficiently induce cell death and TGI in *RB1*-deficient ER<sup>+</sup> breast cancer. In light of the recognized occurrence of *RB1* loss in some ER<sup>+</sup> breast cancers following clinical progression on CDK4/6i, these findings nominate CFI-402257 as a candidate biomarker-directed therapeutic strategy in this setting. Moreover, these data suggest that in addition to loss of *RB1*, markers of impaired *RB1* checkpoint could be used as a more general predictive biomarker for CFI-402257 in breast cancer.

### CFI-402257 potentiates chromosome missegregation and DNA damage in genomically unstable CDK4/6i-resistant breast cancer models

To study the effects of CFI-402257 treatment on different CDK4/6i-resistant models, we selected representative cell lines from our panel of Palbo-R (T47D) and *RB1* loss (MCF7) models and performed live-cell microscopy to analyze mitotic progression for up to 24 hours after addition of the inhibitor to the medium. As expected, and consistent with our previous characterization (33, 36), TTK inhibition by CFI-402257 (150 nM) induced premature segregation and reduced the time cells spent in mitosis (Fig. 4A). This reduction was similar across all tested parental and resistant cell lines (1.5- to 1.7-fold reduction). Because no differences were observed between CDK4/6i-resistant and parental models regarding the shortening of mitosis induced by CFI-402257, we then hypothesized that the outcomes of mitosis, and not the duration, may explain differences in CFI-402257 sensitivity between these models. To test this, we analyzed the segregation errors induced by CFI-402257 in these cell lines. T47D and MCF7 parental lines exhibited different types of mitotic aberrations when exposed to CFI-402257, likely due to different genomic backgrounds (Fig. 4B). While CFI-402257 mainly caused mild segregation errors (i.e., micronuclei, anaphase bridges, and lagging chromosomes) in T47D, the main effect on MCF7 was early mitotic exit without segregation. Despite these phenotypic differences between the parental cell lines, T47D Palbo-R and MCF7 *RB1*<sup>-/-</sup> showed a higher incidence of severe segregation errors (i.e., multiple micronuclei, thick anaphase bridges, asymmetric segregation, multipolar spindles, and multinucleated cells) compared to their matched parental lines upon treatment. To analyze the effect of CFI-402257 on genomic instability after longer treatment times, we scored the incidence of micronuclei following 48 hours of continuous treatment in two Palbo-R and two *RB1*<sup>-/-</sup> cell lines. Consistent with the segregation errors observed by live-cell microscopy, Palbo-R and *RB1*<sup>-/-</sup> cells accumulated a higher number of micronuclei after 48 hours of CFI-402257 treatment than matched parental cells (Fig. 4, C and D). This treatment-induced potentiation of genomic instability was accompanied by an increase in  $\gamma$ H2AX in all tested Palbo-R and *RB1*<sup>-/-</sup> cell lines and PDO (Fig. 4, E and F, and fig. S6A). Collectively, these experiments demonstrate that premature segregation caused by CFI-402257 induces more severe mitotic phenotypes in Palbo-R and *RB1*<sup>-/-</sup> preclinical

models compared to parentals, which drive higher levels of DNA damage and genomic instability.

Last, and given the association between genomic instability and induction of an innate immune signaling described in other settings (40), we asked whether CFI-402257 could induce a tumor cell-intrinsic interferon response in Palbo-R and *RB1*<sup>-/-</sup> cells. CFI-402257 was able to induce STAT1 (signal transducer and activator of transcription 1) phosphorylation, a bona fide marker of type I interferon pathway activation, in most of the ER<sup>+</sup> breast cancer cell lines, although the relative induction in Palbo-R versus parental lines was variable across models (fig. S6B). Despite the variability in the Palbo-R panel, CFI-402257 consistently increased pSTAT1 levels in *RB1*<sup>-/-</sup> cell lines to a greater extent compared to their parental controls (fig. S6C). Activation of cancer cell-intrinsic interferon response was validated by analyzing the expression of a panel of genes involved in type I interferon signaling in representative models of Palbo-R (T47D) and *RB1* loss (CAMA1) (Fig. 4G and fig. S6D). Therefore, these results suggest that CFI-402257 treatment may activate the immune checkpoint in CDK4/6i-resistant ER<sup>+</sup> breast cancers, especially those with *RB1* loss.

Together, our data suggest that a subset of CDK4/6i-resistant ER<sup>+</sup> breast cancers that accumulate mitotic errors and genomic instability, through either *RB1* loss or alternative mechanisms, acquire an enhanced sensitivity to the TTKi CFI-402257 (Fig. 4H). Paralleling what is described in triple-negative breast cancers that are prone to mitotic abnormalities, in this newly defined subset of ER<sup>+</sup> breast cancers, inactivation of the SAC and premature chromosome segregation caused by CFI-402257 leads to intolerable levels of genomic instability and cell death, triggering a tumor cell-intrinsic immune response. This creates an exploitable therapeutic vulnerability and nominates CFI-402257 as a potential therapy for CDK4/6i-resistant ER<sup>+</sup> breast cancer that is characterized by *RB1* loss and/or high genomic instability.

## DISCUSSION

Drug resistance is a universal problem in the treatment of metastatic solid tumors. The development of resistance to CDK4/6i treatment ultimately limits the clinical impact of this important class of therapy for ER<sup>+</sup> breast cancer, which is now used widely as standard initial treatment of metastatic disease. The clinical success of CDK4/6i in this setting has stimulated their evaluation in earlier stage disease and other disease settings, including ER<sup>+</sup>/HER2<sup>+</sup> breast cancer, and selected solid tumors of different origins (e.g., melanoma, pancreas, and hepatic, among others) (41–44). The rapid implementation of these treatments and the clear evidence that effective therapy shapes subsequent tumor evolution emphasize the urgent need to characterize and understand the therapeutic vulnerabilities of CDK4/6i-resistant tumors such that successive lines of therapy can be most rationally designed. Current standards include other endocrine therapies, investigational targeted therapies, or chemotherapy regimens, which are not specifically linked to the biology of CDK4/6i-resistant disease. As a consequence, empiric clinical evaluation of treatments in unselected patients is prone to failure, and biomarker-informed strategies that specifically target vulnerabilities of the resistance state are of interest.

Our studies have revealed an accumulation of mitotic errors and micronuclei in a subset of preclinical models of ER<sup>+</sup> breast cancer with acquired resistance to the CDK4/6i palbociclib (Fig. 1). *RB1* loss, a common mechanism of CDK4/6i resistance, is known to induce

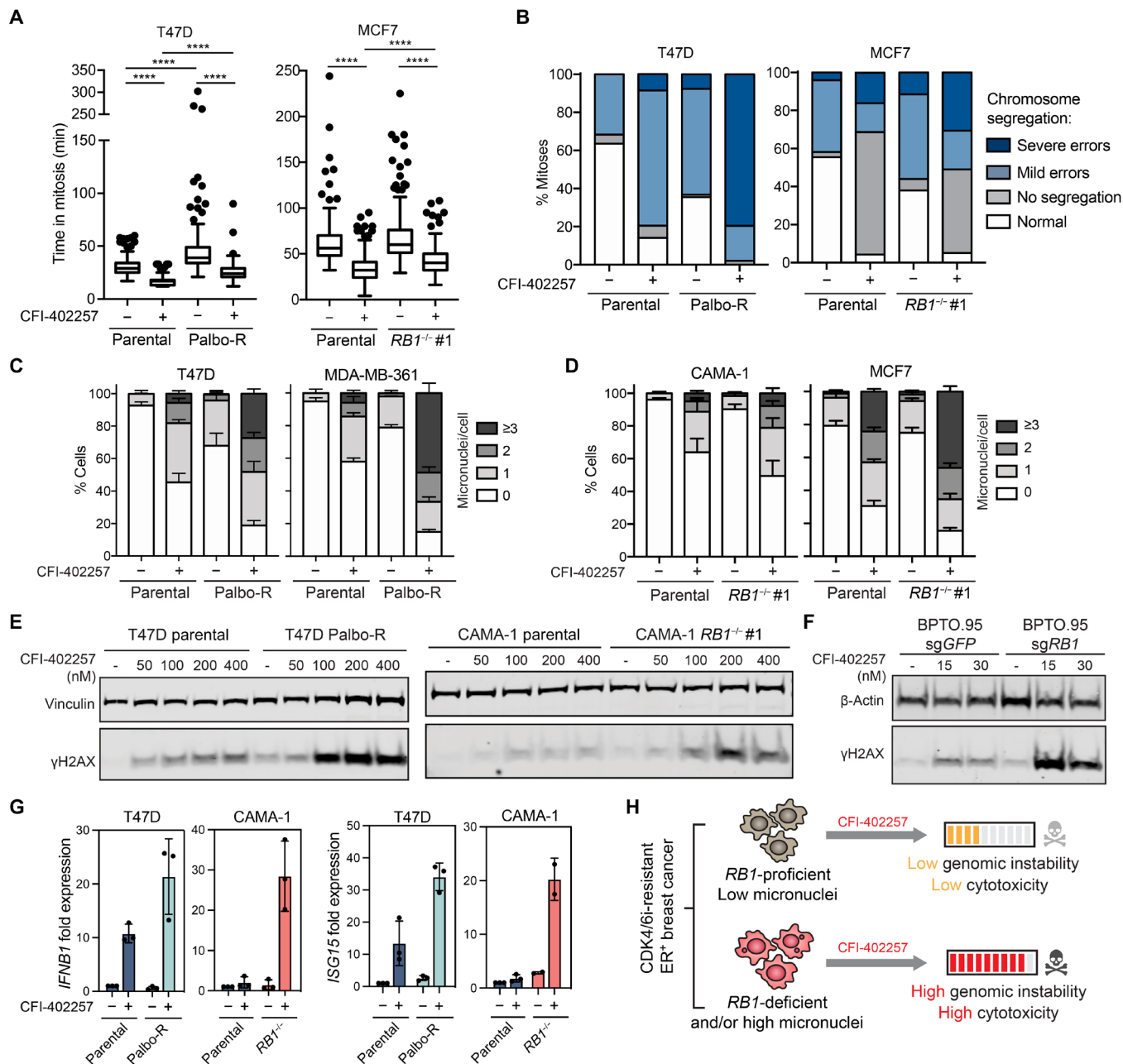


**Fig. 4. Genomic instability induced by CFI-402257 is potentiated in CDK4/6i-resistant breast cancer.** (A) Duration of mitosis in representative Palbo-R (T47D) and *RB1*<sup>-/-</sup> (MCF7) lines treated with 150 nM CFI-402257, measured by live-cell imaging. Pooled data from two independent experiments are plotted. Kruskal-Wallis non-parametric test, Dunn's multiple comparison, \*\*\*\**P* < 0.0001. (B) Classification of mitotic phenotypes observed in (A). (C and D) Immunofluorescence-based analysis of micronuclei incidence in Palbo-R (C) and *RB1*<sup>-/-</sup> (D) cells treated with 150 nM CFI-402257 for 48 hours. Mean ± SD of three independent experiments is shown, and 200 cells were counted per condition in each experiment. (E and F) DNA damage induced by CFI-402257 demonstrated by γH2AX immunoblot in Palbo-R and *RB1*<sup>-/-</sup> cell lines treated for 72 hours (E) and *RB1*-deficient PDO treated for 12 days (F). (G) RT-qPCR analysis of expression of *IFNB1* and *ISG15* after CFI-402257 treatment in selected Palbo-R and *RB1*<sup>-/-</sup> cell lines by RT-qPCR. Cells were treated with 150 nM CFI-402257 for 72 hours. Data for Palbo-R and *RB1*<sup>-/-</sup> models are presented as relative expression to that in matched parentals treated with DMSO. (H) Model of induced sensitivity to CFI-402257. Two general categories of CDK4/6i-resistant tumors are identified according to their accumulation of genomic instability. In *RB1*-proficient cells with low micronuclei incidence, CFI-402257 treatment causes low levels of genomic instability that are manageable for the cells. In CDK4/6i-resistant ER<sup>+</sup> breast cancer cells with *RB1* loss and/or high incidence of micronuclei, CFI-402257 treatment leads to intolerable levels of genomic instability, causing cell death.

these phenotypes (34). However, our results demonstrate that, in addition to *RBI* loss, alternative mechanisms of resistance that retain intact Rb expression can also converge in the accumulation of genomic instability and enhance tumor cell sensitivity to mitotic kinase inhibitors (Fig. 2) known to potentiate genomic instability to intolerable levels (45). In addition to the mitotic aberrations we identified in a subset of models, we noticed that most of our CDK4/6i-resistant models had increased levels of endogenous DNA damage (measured by H2AX phosphorylation). In line with these results, Kettner *et al.* (25) reported increased evidence of DNA damage in palbociclib-resistant MCF7 and T47D cell lines and post-palbociclib ER<sup>+</sup> breast cancer patient samples. In addition, Crozier *et al.* (31) have demonstrated that short-term treatment with CDK4/6i induces replication stress and genomic instability in RPE1 cells. These findings suggest that the prolonged inhibition of CDK4/6i activity and/or the mechanisms that allow cells to escape from CDK4/6i inhibition can lead to molecular alterations and phenotypes—i.e., *RBI* loss, high incidence of mitotic aberrations, and endogenous DNA damage—that were not characteristic of ER<sup>+</sup> breast tumors before the adoption of CDK4/6i therapies, but are frequently found in highly genomically unstable tumors, typically triple-negative breast cancers. This switch in molecular subtype and the accumulation of genomic instability have also been reported in patients treated with palbociclib at the time of progression treatment (24, 25). Accordingly, therapies that historically have attempted to leverage genomic instability characteristic of triple-negative breast cancers, such as poly(ADP-ribose) polymerase (PARP) and mitotic kinase inhibitors, may have newfound application in CDK4/6i-resistant ER<sup>+</sup> breast tumors.

The kinase TTK, also known as monopolar spindle 1 (MPS1), is a key regulator of the mitotic SAC and an example of a target that was initially not considered for ER<sup>+</sup> breast cancer. TTK-dependent SAC activation contributes to the maintenance of genome stability by delaying chromosome segregation (i.e., anaphase) until all chromosomes are properly attached to the mitotic spindle in metaphase (46). Once this is achieved, the checkpoint is satisfied, TTK becomes inactive, and cells progress to anaphase. Consequently, pharmacologic inactivation of the SAC by TTKi such as CFI-402257 induces premature chromosome segregation, leading to aneuploidy, genomic instability, and cell death (33, 47–51).

Initial preclinical investigation of TTKi demonstrated increased activity in tumors with high levels of genomic instability (33, 52, 53). However, as CDK4/6i have only recently been incorporated into standard therapy, models of CDK4/6i resistance could not be and were not considered. By developing the models used here, we generated a platform specifically relevant to the investigation of this important and emerging clinical context. Using these models, we found that CDK4/6i-resistant breast cancers with elevated mitotic aberrations relative to their parental CDK4/6i-sensitive derivatives were hypersensitive to TTK inhibition. Furthermore, our data indicate that the abundance of micronuclei and gene signatures of *RBI* loss of function represent promising predictive biomarkers of response to the TTKi CFI-402257. Rather than directly causing CFI-402257 sensitivity, we hypothesize that the presence of micronuclei is indicative of underlying chromosome segregation errors and could be used to identify cancer cells [in solid or liquid biopsies following CDK4/6i progression, or perhaps in circulating tumor cells (54)] that rely on SAC activation to maintain tolerable levels of genomic instability. On the other hand, models with elevated levels of endogenous DNA damage without mitotic defects/micronuclei did not exhibit TTKi sensitization.

We report here that *RBI* loss—a recurrent alteration that arises with the development of CDK4/6i resistance—enhances sensitivity to TTK inhibition (Fig. 3). Related to this finding, Gong *et al.* (27) and Oser *et al.* (28) demonstrated that a synthetic lethal interaction exists between *RBI* loss and Aurora kinase A/B inhibition. We found similarities in the drug sensitivity profiles of Palbo-R models to CFI-402257, barasertib, alisertib, and tozasertib (Fig. 2 and fig. S4, A and C), suggesting that the underlying mitotic aberrations sensitize the cells to TTK and Aurora kinase inhibitors. However, the cellular consequences of TTK inhibition demonstrated here differ from the mechanisms that have been described for Aurora kinase inhibitors. In the presence of an activated SAC in *RBI*-deficient cells, inhibition of Aurora kinases A and B causes an indefinite arrest in mitosis that ultimately leads to mitotic catastrophe (27, 28). In contrast, we have demonstrated that TTKi causes an accumulation of genomic instability in *RBI*-deficient cells due to premature chromosome segregation, which is not sustainable for cell survival (Fig. 4). In addition to the different consequences observed in these sensitive models, TTK and Aurora kinase inhibitors exhibit different tolerability profiles, which may affect their therapeutic index or clinical applications—especially in the context of second-line therapy for metastatic ER<sup>+</sup> breast cancer.

Sensitization to CFI-402257 in models of CDK4/6i resistance was observed in both p53 wild-type (e.g., MCF7, KPL-1, and LY2 *RBI*<sup>-/-</sup>, LY2 Palbo-R) and p53 mutant (e.g., T47D and MDA-MB-361 Palbo-R, CAMA-1 *RBI*<sup>-/-</sup>) cell lines, suggesting that p53 status is not a determinant of CFI-402257 sensitization. Previous studies have reported contradictory data regarding p53 requirement for TTKi-induced cell growth inhibition and apoptosis, and suggest that these effects may be inhibitor specific and tumor context dependent (48, 51, 55, 56). Although we have not compared isogenic p53 cell lines, we observe high apoptotic levels in p53-mutated MDA-MB-361 Palbo-R and CAMA-1 *RBI*<sup>-/-</sup>, demonstrating the efficacy of CFI-402257 in p53-deficient tumors (Figs. 2D and 3F and fig. S5H). In addition, CFI-402257 had profound *in vivo* antitumor activity in xenografts derived from p53-proficient MCF7 *RBI*<sup>-/-</sup> cells. Although mechanisms of cell death or growth inhibition may vary, these data suggest that p53 status may not affect CFI-402257 efficacy in CDK4/6i-resistant ER<sup>+</sup> breast cancer.

Consistent with recognized effects of the DNA damage and micronuclei induced by CFI-402257 treatment, we have observed activation of the type I interferon pathway in Palbo-R and *RBI*<sup>-/-</sup> ER<sup>+</sup> breast cancer cell lines after treatment (Fig. 4). Similarly, we have previously reported that the combination of CFI-402257 and PD-1 blockade induces complete tumor regression in syngeneic colon carcinoma CT26 xenografts, suggesting that CFI-402257 can trigger an interferon response and immune checkpoint in this *in vivo* model (33). Although ER<sup>+</sup> breast cancer patients have not been considered as a target population for immunotherapy in the past, these treatments are gaining importance in the clinical context of CDK4/6i resistance. Multiple preclinical and clinical data demonstrate interferon signaling and immune checkpoint activation by CDK4/6i treatment and correlation with intrinsic and acquired CDK4/6i resistance (57, 58). Accordingly, efforts are underway to evaluate immunotherapy in CDK4/6i-resistant disease (ClinicalTrials.gov ID: NCT03147287, NCT04895358). Although we recognize the limitations of *in vitro* models to study cancer immunity, the observation of a cancer cell–intrinsic interferon response in our CDK4/6i-resistant models, which is potentiated by CFI-402257, suggests that further

consideration of antitumor immunity is deserved as CFI-402257 is evaluated in this clinical context.

Given the heterogeneity of potential mechanisms of resistance to CDK4/6i, alternative therapeutic approaches are being developed to target subsets of CDK4/6i-resistant tumors with distinct characteristics. For instance, emerging data suggest that resistant tumors with up-regulated CDK6 expression may benefit from further targeting CDK6 protein stability (59). In another line of study, activation of PI3K/mammalian target of rapamycin (mTOR) signaling pathway is found in CDK4/6i-resistant tumors, and targeted inhibitors of this pathway are being evaluated in combination with endocrine therapy and CDK4/6i to delay emergence of resistance (60, 61). These alterations, as well as the genomic instability and segregation errors we describe here, may define distinct resistant populations that can inform complementary therapeutic strategies. Such efforts will benefit from ongoing studies attempting to characterize predictors and anticipate trajectories of different modes of acquired resistance (62).

In summary, our data demonstrate that mitotic kinase inhibitors, and in particular the selective TTKi CFI-402257, have enhanced antitumor activity in a subset of preclinical CDK4/6i-resistant ER<sup>+</sup> breast cancer models characterized by high levels of micronuclei and mitotic segregation errors. Accordingly, an expansion of the phase 1 clinical trial of CFI-402257 is evaluating the clinical activity of TTK inhibition in patients with ER<sup>+</sup> breast cancer with acquired resistance to CDK4/6i (ClinicalTrials.gov ID: NCT02792465). In an initial report, durable objective responses were recorded in 4 patients (of 10 enrolled) with metastatic ER<sup>+</sup> breast cancer resistant to CDK4/6i and endocrine therapy who received CFI-402257 on a daily oral schedule at doses that were safe and tolerable (63). Correlative evaluation of measures of genomic instability (e.g., micronuclei) and somatic loss of *RB1* in this trial and future clinical studies will provide an opportunity to validate the clinical relevance of our findings and inform the utility of these as selection biomarkers for CFI-402257. However, as our preclinical results demonstrate, contemporaneous sampling of CDK4/6i-resistant disease for correlative analysis will be essential to capture the correlates of therapy-induced TTKi sensitivity. As *RB1* loss can be detected in circulating tumor DNA (ctDNA) at the time of CDK4/6i resistance, liquid biopsy-based correlative and/or enrichment trials provide an attractive means to address the challenges imposed by the need for fresh biopsy (64). Our findings therefore provide a clinically tractable, rationally designed approach to stratified treatment that specifically addresses vulnerabilities that accompany CDK4/6i resistance. If validated clinically, such an approach would have immense potential to improve the outcomes for this most common and ever-expanding cohort of patients with metastatic cancer, by providing a novel line of therapy to target the resistant state.

## MATERIALS AND METHODS

### Study design

This study aimed to investigate the accumulation of genomic instability and chromosome segregation errors after acquisition of resistance to CDK4/6i in ER<sup>+</sup> breast cancer and to test the efficacy of mitotic kinase inhibitors as a potential treatment for CDK4/6i-resistant breast cancer patients. To this end, we generated diverse laboratory models of CDK4/6i resistance through palbociclib dose escalation or through CRISPR-mediated *RB1* knockout in breast

cancer cell lines and PDOs. Genomic instability was measured by micronuclei formation, and chromosome missegregation was visualized by live-cell imaging. Multiple mitotic kinase inhibitors were tested in these models, including our TTKi, CFI-402257. Sensitivity to these treatments was analyzed by dose-response assays. The effects of CFI-402257 treatment were analyzed by measuring apoptosis, DNA damage, genomic instability, and triggering of interferon response. In vivo efficacy of CFI-402257 in breast cancer models with *RB1* loss was analyzed by treating female SCID mice harboring *RB1*<sup>-/-</sup> or wild-type MCF7-derived tumors. The number of mice used in each experimental group was determined on the basis of statistical power analysis and equaled six mice per arm. Before treatment, mice were randomized on the basis of tumor volume to ensure evenly distributed average tumor sizes across each group. For all other experiments, at least two independent biological replicates were performed. Sample size, number of replicates, and statistical methods are indicated in the figure legends when relevant. For experiments in which technical replicates were used [i.e., reverse transcription quantitative polymerase chain reaction (RT-qPCR) and cell survival in dose-response assays], outliers were excluded from the analysis when their standard variation value within one group of technical replicates was greater than 0.3. Experimenters were not blinded during the study.

### Cell lines and PDOs

Breast cancer cell lines were gifts from B. Neel. Short tandem repeat (STR) profiling was used to verify authenticity of the cell lines. Sixteen STR loci were simultaneously amplified in multiplex PCR at The Center for Applied Genomics at SickKids Hospital (Toronto), and the American Type Culture Collection database was used for comparison when possible. For PDOs, primary tumor tissue was collected with informed patient consent and University Health Network (UHN) Research Ethics Board approval (17-5518). The tissue was minced and digested in advanced Dulbecco's modified Eagle's medium/F12 containing 1× GlutaMAX, 10 mM HEPES, and 1× antibiotic-antimycotic (AdDF+++), with Liberase TH (500 µg/ml) for 1 hour at 37°C, followed by passage over a 100-µm cell strainer, treatment with red cell lysis buffer, and centrifugation. Cells were counted and plated at a density of 80,000 cells per well in 50 µl of basement membrane extract (BME) domes in 24-well plates. Once the BME domes had solidified for 10 to 15 min, they were overlaid with breast organoid medium, as previously described (65). The medium was changed every 3 to 4 days, and organoids were passaged with TrypLE Express as previously detailed (65). Organoids were confirmed to match the original patient tissue by STR analysis and were verified to be of tumor origin by pathology review and by single-nucleotide polymorphism (SNP) analysis. Organoids were embedded in HistoGel and formalin-fixed for histology. Paraffin embedding and immunohistochemistry were completed by the UHN Drug Development Program Biomarker Laboratory. Cells and organoids were routinely tested for mycoplasma.

### Generation of acquired resistance to palbociclib in cell lines and organoids

Palbociclib resistance was developed by continuous dose escalation of palbociclib up to 0.5 to 1 µM until cell growth was observed in the presence of the drug (6 to 8 months for cell lines and 10 to 12 months for PDO). During this time, parental cell lines and organoids were cultured in regular medium to match the time spent in culture. Once resistance was established, Palbo-R cell lines and PDO were

cultured in regular growth medium without palbociclib. Cells were cultured without palbociclib for at least 2 weeks before evaluating resistance. STR profiling was performed after establishing resistance to confirm cell identity matching between Palbo-R and parental pairs.

### RB1 gene editing

*RB1*<sup>-/-</sup> cell lines were generated by transient transfection of cells with pX330 plasmid (Addgene, #110403) containing a single-guide RNA targeting *RB1* (AGAGCAGGACAGCGGCCCGG), followed by a 24-hour pulse of puromycin selection. Individual clones of cells were selected and screened for Rb expression. *RB1* gene editing in PDO was performed by lentiviral transduction of lentiCRISPR v2 plasmid (Addgene, #52961) containing the same sg*RB1* sequence used for cell lines or sg*GFP* (GGGCGAGGAGCTGTTCACCG), followed by puromycin selection. A polyclonal population was used for experiments. Rb protein loss was confirmed by immunoblotting. PDOs were also subjected to Rb immunohistochemistry.

### Growth curves

*RB1*<sup>-/-</sup> and parental cell lines were seeded in 24-well plates at 5 to 10% confluency. Cells were imaged (four fields per well) every 4 hours for 5 days using an IncuCyte system (Sartorius) with a ×4 magnification objective, and confluency was calculated for each well and time point. Growth rate and doubling time were calculated using confluency data at the final and initial time points.

### Exome sequencing

Genomic DNA was extracted from parental and Palbo-R cells and organoids using a NucleoSpin Tissue kit (Macherey-Nagel). Agilent SureSelect All Exon V5 probes were used for hybrid selection to prepare whole-exome sequencing libraries according to manufacturing protocol. Libraries were then sequenced with paired-end reads of 125 base pairs on Illumina HiSeq 2500. Median coverage of 90× was achieved. Raw sequencing reads were aligned to the hg38 human genome using bwa-mem (v0.7.17). Duplicates were marked using Picard (v2.26.0), and local realignment was performed using GATK (v3.8) (<https://github.com/Cesconlab/ExomeSeq>).

### Mutation calling

Somatic single-nucleotide variants and small insertion and deletion were identified using four different callers: MuTect (v1.1.5), MuTect2 (GATK v3.8), Strelka (v2.9.10), and VarScan2 (v2.4.4). Somatic mutations from each caller were then compared using bcftools (v1.15.1). Alterations called by at least two callers were further filtered to remove regions of poor mappability (66) (<https://github.com/Cesconlab/ExomeSeq>).

### Copy number

We sequenced DNA for shallow whole-genome sequencing (sWGS) to a mean coverage of 0.5×. Sequenced data were aligned to the human genome reference hg38 using bwa-mem (v0.7.17), and duplicates were marked and removed using GATK (v3.8). CN profiles were determined using the R package IchorCNA (<https://github.com/Cesconlab/sWGS>). CN profiles were stratified using log<sub>2</sub> ratio (LR) with negative values being deletion and positive being amplification as follows: shallow < |0.5|, deep > |1|.

### Genomic alteration analysis

Parental and resistant mutations were merged separately, and resistant exclusive mutations were identified using bedtools intersect. Similarly,

alterations of CN profiles in resistance compared to parental samples were identified by analyzing the difference in LR and differential CN segments were annotated using GISTIC2. By focusing on genes involved in CDK4/6i resistance, functional mutations were annotated using VEP (v98) and plotted using the R package maftools. Given the high rate of mutation found in *FAT1*, we focused our analysis on mutations identified by Li *et al.* (15).

### Xenograft tumor growth

Parental or *RB1*<sup>-/-</sup> MCF7 cells (10<sup>7</sup>) were mixed with Matrigel matrix (Sigma-Aldrich) in a 1:1 ratio (total volume of 100 μl) and injected subcutaneously in female severe combined immunodeficient (SCID) mice. Before establishing xenografts, 17β-estradiol pellets (0.35 mg, 60-day release, Innovative Research of America) were implanted subcutaneously in the mice. When the tumors reached an average volume of 100 mm<sup>3</sup>, mice were randomized between treatment groups. Mice received control vehicle (90% Kollisolv PEG E 400, Sigma-Aldrich) or CFI-402257 at the indicated doses and schedules by oral gavage (*n* = 6 mice per treatment group). Tumors were measured with digital calipers, and tumor volume (*V*) was calculated as  $V = (\text{length} \times \text{width}^2)/2$ . Body weight of each mouse was recorded every 2 to 3 days. Xenograft studies were designed and conducted following the institutional animal care guidelines, according to a protocol approved by the UHN Animal Care Committee.

### Drug dose-response assays

Response to palbociclib was evaluated by colony survival (cell lines, except MDA-MB-361, which does not grow well in colonies), sulforhodamine-B (SRB) assay (MDA-MB-361), or Presto Blue assay (BPTO.95 PDO). IC<sub>50</sub> values for palbociclib were calculated using the methodology that was more appropriate for each model. Abemaciclib response was evaluated by SRB assay (cell lines) or Presto Blue assay (BPTO.95 PDO). Mitotic kinase inhibitors (CFI-402257, barasertib, alisertib, tozasertib, volasertib, and RO-3306) were evaluated by SRB assay (cell lines) or Presto Blue assay (BPTO.95 PDO). For palbociclib colony survival assays, cells were sparsely seeded in six-well plates and treated with the indicated doses of palbociclib or mock-treated for 12 to 14 days. Colonies were then stained with SRB and counted. For SRB assays, cells were plated in 96-well plates (cell lines treated with mitotic kinase inhibitors) or 24-well plates (cell lines treated with abemaciclib and MDA-MB-361 cells treated with palbociclib) and treated with serial drug dilutions for 5 days (mitotic kinase inhibitors) or 14 days (palbociclib and abemaciclib). Cells were then fixed, stained with SRB, and solubilized, and absorbance was quantified on a spectrophotometer. For Presto Blue assays, PDOs were dissociated and 2000 cells per well were plated in 48-well plates in 25-μl BME domes. Once BME had solidified, the domes were overlaid with organoid medium containing the indicated concentrations of drugs. After 12 to 14 days, the medium was removed and replaced by 1× PrestoBlue HS Reagent in breast organoid medium and incubated overnight at 37°C and 5% CO<sub>2</sub>. The next day, aliquots of medium supernatants were measured by fluorescence using a Clariostar instrument.

AAC was calculated for mitotic kinase inhibitors using the PharmacoGx pipeline (67).

CFI-402257 was synthesized as described previously (68), MPI-0479605 was synthesized by HDH Pharma, and NMS-P715 was synthesized by Sundia. Palbociclib and abemaciclib were purchased from Medkoo, RO-3306 from Cedarlane, barasertib (AZD1152-hydroxyquinazoline) and alisertib (MLN8237) from AstaTech,

tozasertib (VX-680) from Sundia MediTech Company, and volasertib (BI-6727) from Chemietek.

### Immunoblotting

Cells were lysed in SDS sample buffer [62.5 mM tris-HCl (pH 6.8), 2% SDS, and 10% glycerol] supplemented with benzoinase (Sigma-Aldrich). Samples were then subjected to standard SDS–polyacrylamide gel electrophoresis and immunoblotting following LI-COR recommendations for imaging with an Odyssey CLx system.

Primary antibodies are as follows: mouse anti-Rb (Cell Signaling Technology, 9309), rabbit anti-actin (Sigma-Aldrich, SAB5600204), rabbit anti-vinculin (Cell Signaling Technology, 13901), mouse anti-p53 (Santa Cruz Biotechnology, sc-47698), mouse anti-p21 (Santa Cruz Biotechnology, sc-6246), rabbit anti- $\gamma$ H2AX (Cell Signaling Technology, 9718), rabbit cleaved caspase-3 (Cell Signaling Technology, 9661), rabbit anti-pSTAT1 Tyr<sup>701</sup> (Cell Signaling Technology, 9167), mouse anti-phospho-histone H3 Ser<sup>10</sup> (Cell Signaling Technology, 9706), and rabbit histone H3 (Cell Signaling Technology, 4499). Secondary antibodies are as follows: goat anti-mouse immunoglobulin G (IgG) IRDye 800CW (LI-COR, 926-32210) and goat anti-rabbit IgG (H+L) Alexa Fluor 594 (Thermo Fisher Scientific, A32740).

### Reverse transcription quantitative polymerase chain reaction

Standard RT-qPCR methods based on SYBR Green detection were used to analyze the expression of genes related to CDK4/6i resistance in Palbo-R and parental models, and genes of the type I interferon pathway in CFI-402257-treated cell lines. Sequences of the primers are included in table S4.

### Live-cell, time-lapse microscopy

Cell lines and PDO were plated in LabTek chamber slides and incubated with SiR-DNA stain (Cytoskeleton; 333 nM for cell lines and 1  $\mu$ M for PDO) for 2 hours before imaging. For live-cell experiments with CFI-402257 treatment, 150 nM CFI-402257 or dimethyl sulfoxide (DMSO) was coadded to the medium with SiR-DNA. Cells were held in a humidified Chamlide stage incubator kept at 37°C and 5% CO<sub>2</sub> (Live Cell Instrument). Time-lapse images were captured using Volocity 6.3 software (Quorum Technologies) on a Quorum WaveFX spinning disk confocal microscope (Quorum Technologies) equipped with a Hamamatsu ImageEM electron-multiplying charge-coupled device camera at  $\times 20$  magnification every 4 min for 20 to 24 hours. The time from nuclear envelope breakdown to mitotic exit (i.e., anaphase or chromatin decondensation) was recorded for each dividing cell. For all dividing cells, mitoses were scored as normal, mild segregation errors (i.e., micronuclei, anaphase bridges, and lagging chromosomes), severe segregation errors (i.e., several micronuclei, thick anaphase bridges, asymmetric segregation, multipolar spindles, and multinucleated cells), and mitotic exit without segregation.

### Micronuclei detection

To detect micronuclei, cells were plated on coverslips, fixed, probed with mouse anti- $\alpha$ -tubulin antibody (Sigma-Aldrich, T9026) and Cy2 AffinityPure donkey anti-mouse IgG (Jackson ImmunoResearch) to detect cell boundaries, and stained with 4',6-diamidino-2-phenylindole (DAPI) (Sigma-Aldrich). Mounted coverslips were imaged on a Zeiss AxioImager upright microscope equipped with a scientific

complementary metal-oxide semiconductor (sCMOS) camera at  $\times 63$  magnification.

### Apoptosis assay

Drug-induced apoptosis was assessed by annexin V combined with propidium iodide (PI) staining. Cells and supernatants were collected following treatment and stained with annexin V–fluorescein isothiocyanate at 2.25  $\mu$ g/ml (BioLegend) and PI at 10  $\mu$ g/ml (Sigma-Aldrich) and measured on a BD FACSCanto II flow cytometer.

### RB1-loss scores

To calculate RB1-loss scores in the panel of breast cancer cell lines, we selected three independently generated gene lists consisting of genes that are up-regulated or down-regulated in RB1-deficient context (37–39). Breast cancer cell line gene expression profiles were obtained from Marcotte *et al.* (69). Eguchi and Knudsen signatures included only genes that were up-regulated after RB1 loss, and scores were calculated as the average fragments per kilobase of exon per million mapped fragments (FPKM) of genes included in the lists. Vernell signature included genes that were either up- or down-regulated after RB1 loss, and the score was calculated by subtracting the average FPKM of down-regulated genes from the average FPKM of up-regulated genes.

### Statistical analyses

Prism software (GraphPad Software LLC) was used for statistical analysis. Statistical tests used for each experiment and number of replicates are indicated in the corresponding figure legends. For all statistics,  $P < 0.05$  was considered significant.

### SUPPLEMENTARY MATERIALS

Supplementary material for this article is available at <https://science.org/doi/10.1126/sciadv.abq4293>

### REFERENCES AND NOTES

1. Y. Gong, Y.-R. Liu, P. Ji, X. Hu, Z.-M. Shao, Impact of molecular subtypes on metastatic breast cancer patients: A SEER population-based study. *Sci. Rep.* **7**, 45411 (2017).
2. J. L. Caswell-Jin, S. K. Plevritis, L. Tian, C. J. Cadham, C. Xu, N. K. Stout, G. W. Sledge, J. S. Mandelblatt, A. W. Kurian, Change in survival in metastatic breast cancer with treatment advances: Meta-analysis and systematic review. *JNCI Cancer Spectr.* **2**, ky062 (2018).
3. C. Bertoli, J. M. Skotheim, R. A. M. de Bruin, Control of cell cycle transcription during G1 and S phases. *Nat. Rev. Mol. Cell Biol.* **14**, 518–528 (2013).
4. K. L. Thu, I. Soria-Bretones, T. W. Mak, D. W. Cescon, Targeting the cell cycle in breast cancer: Towards the next phase. *Cell Cycle* **17**, 1871–1885 (2018).
5. R. S. Finn, J. Dering, D. Conklin, O. Kalous, D. J. Cohen, A. J. Desai, C. Ginther, M. Atefi, I. Chen, C. Fowst, G. Los, D. J. Slamon, PD 0332991, a selective cyclin D kinase 4/6 inhibitor, preferentially inhibits proliferation of luminal estrogen receptor-positive human breast cancer cell lines in vitro. *Breast Cancer Res.* **11**, R77 (2009).
6. M. Cristofanilli, N. C. Turner, I. Bondarenko, J. Ro, S.-A. Im, N. Masuda, M. Colleoni, A. DeMichele, S. Loi, S. Verma, H. Iwata, N. Harbeck, K. Zhang, K. P. Theall, Y. Jiang, C. H. Bartlett, M. Koehler, D. Slamon, Fulvestrant plus palbociclib versus fulvestrant plus placebo for treatment of hormone-receptor-positive, HER2-negative metastatic breast cancer that progressed on previous endocrine therapy (PALOMA-3): Final analysis of the multicentre, double-blind, phase 3 randomised controlled trial. *Lancet Oncol.* **17**, 425–439 (2016).
7. S.-A. Im, Y.-S. Lu, A. Bardia, N. Harbeck, M. Colleoni, F. Franke, L. Chow, J. Sohn, K.-S. Lee, S. Campos-Gomez, R. Villanueva-Vazquez, K.-H. Jung, A. Chakravarty, G. Hughes, I. Gounaris, K. Rodriguez-Lorenc, T. Taran, S. Hurvitz, D. Tripathy, Overall survival with ribociclib plus endocrine therapy in breast cancer. *N. Engl. J. Med.* **381**, 307–316 (2019).
8. N. C. Turner, D. J. Slamon, J. Ro, I. Bondarenko, S.-A. Im, N. Masuda, M. Colleoni, A. DeMichele, S. Loi, S. Verma, H. Iwata, N. Harbeck, S. Loibl, F. André, K. Puyana Theall, X. Huang, C. Giorgetti, C. Huang Bartlett, M. Cristofanilli, Overall survival with palbociclib and fulvestrant in advanced breast cancer. *N. Engl. J. Med.* **379**, 1926–1936 (2018).
9. D. J. Slamon, P. Neven, S. Chia, P. A. Fasching, M. De Laurentiis, S.-A. Im, K. Petrakova, G. V. Bianchi, F. J. Esteva, M. Martín, A. Nusch, G. S. Sonke, L. De la Cruz-Merino, J. T. Beck, X. Pivot, M. Sondhi, Y. Wang, A. Chakravarty, K. Rodriguez-Lorenc, T. Taran, G. Jerusalem,

- Overall survival with ribociclib plus fulvestrant in advanced breast cancer. *N. Engl. J. Med.* **382**, 514–524 (2020).
10. S. Johnston, M. Martin, A. Di Leo, S.-A. Im, A. Awada, T. Forrester, M. Frenzel, M. C. Hardebeck, J. Cox, S. Barriga, M. Toi, H. Iwata, M. P. Goetz, MONARCH 3 final PFS: A randomized study of abemaciclib as initial therapy for advanced breast cancer. *NPJ Breast Cancer* **5**, 5 (2019).
  11. F. Schettini, F. Giudici, M. Giuliano, M. Cristofanilli, G. Arpino, L. Del Mastro, F. Puglisi, S. De Placido, I. Paris, P. De Placido, S. Venturini, M. De Laurentis, P. Conte, D. Juric, A. Llombart-Cussac, L. Pusztai, A. Prat, G. Jerusalem, A. Di Leo, D. Generali, Overall survival of CDK4/6-inhibitor-based treatments in clinically relevant subgroups of metastatic breast cancer: Systematic review and meta-analysis. *J. Natl. Cancer Inst.* **112**, 1089–1097 (2020).
  12. J. A. O'Shaughnessy, S. Johnston, N. Harbeck, M. Toi, Y.-H. Im, M. Reinisch, Z. Shao, P. L. K. Lehtinen, C.-S. Huang, A. Tryakin, M. Goetz, H. S. Rugo, E. Senkus, L. Testa, M. Andersson, K. Tamura, G. G. Steger, L. Del Mastro, J. Cox, T. Forrester, S. Sherwood, X. Li, R. Wei, M. Martin, P. Rastogi, Abstract GS1-01: Primary outcome analysis of invasive disease-free survival for monarchE: Abemaciclib combined with adjuvant endocrine therapy for high risk early breast cancer. *Cancer Res.* **81**, GS1-01 (2021).
  13. B. O'Leary, R. J. Cutts, Y. Liu, S. Hrebien, X. Huang, K. Fenwick, F. André, S. Loibl, S. Loi, I. Garcia-Murillas, M. Cristofanilli, C. Huang Bartlett, N. C. Turner, The genetic landscape and clonal evolution of breast cancer resistance to palbociclib plus fulvestrant in the PALOMA-3 trial. *Cancer Discov.* **8**, 1390–1403 (2018).
  14. P. Razavi, C. H. dos Anjos, D. N. Brown, L. Qing, C. Ping, J. Herbert, J. Colon, D. Liu, M. Mao, L. Norton, M. Scaltriti, D. B. Solit, M. E. Robson, J. S. Reis-Filho, K. L. Jhaveri, S. Chandralapaty, Molecular profiling of ER<sup>+</sup> metastatic breast cancers to reveal association of genomic alterations with acquired resistance to CDK4/6 inhibitors. *J. Clin. Oncol.* **37**, 1–1009 (2019).
  15. Z. Li, P. Razavi, Q. Li, W. Toy, B. Liu, C. Ping, W. Hsieh, F. Sanchez-Vega, D. N. Brown, A. F. Da Cruz Paula, L. Morris, P. Selenica, E. Eichenberger, R. Shen, N. Schultz, N. Rosen, M. Scaltriti, E. Brogi, J. Baselga, J. S. Reis-Filho, S. Chandralapaty, Loss of the FAT1 tumor suppressor promotes resistance to CDK4/6 inhibitors via the Hippo pathway. *Cancer Cell* **34**, 893–905.e8 (2018).
  16. L. Formisano, Y. Lu, A. Servetto, A. B. Hanker, V. M. Jansen, J. A. Bauer, D. R. Sudhan, A. L. Guerrero-Zotano, S. Croessmann, Y. Guo, P. G. Ericsson, K.-M. Lee, M. J. Nixon, L. J. Schwarz, M. E. Sanders, T. C. Dugger, M. R. Cruz, A. Behdad, M. Cristofanilli, A. Bardia, J. O'Shaughnessy, R. J. Nagy, R. B. Lanman, N. Solovieff, W. He, M. Miller, F. Su, Y. Shyr, I. A. Mayer, J. M. Balko, C. L. Arteaga, Aberrant FGFR signaling mediates resistance to CDK4/6 inhibitors in ER<sup>+</sup> breast cancer. *Nat. Commun.* **10**, 1373 (2019).
  17. R. Condorelli, L. Spring, J. O'Shaughnessy, L. Lacroix, C. Baillieux, V. Scott, J. Dubois, R. J. Nagy, R. B. Lanman, A. J. Iafrate, F. Andre, A. Bardia, Polyclonal RB1 mutations and acquired resistance to CDK 4/6 inhibitors in patients with metastatic breast cancer. *Ann. Oncol.* **29**, 640–645 (2018).
  18. S. A. Wander, O. Cohen, X. Gong, G. N. Johnson, J. Buendia-Buendia, M. R. Lloyd, D. Kim, F. Luo, P. Mao, K. Helvie, K. J. Kowalski, U. Nayyar, A. G. Waks, S. Parsons, R. Martinez, L. M. Litchfield, X. S. Ye, C. P. Yu, V. M. Jansen, J. R. Stille, P. S. Smith, G. J. Oakley, Q. Chu, G. Batist, M. Hughes, J. D. Kremer, L. A. Garraway, E. P. Winer, S. M. Tolaney, N. U. Lin, S. Buchanan, N. Wagle, The genomic landscape of intrinsic and acquired resistance to cyclin-dependent kinase 4/6 inhibitors in patients with hormone receptor positive metastatic breast cancer. *Cancer Discov.* **10**, 1174–1193 (2020).
  19. U. S. Asghar, R. Kanani, R. Roylance, S. Mittnacht, Systematic review of molecular biomarkers predictive of resistance to CDK4/6 inhibition in metastatic breast cancer. *JCO Precis. Oncol.* **6**, e2100002 (2022).
  20. A. L. Manning, N. J. Dyson, RB: Mitotic implications of a tumour suppressor. *Nat. Rev. Cancer* **12**, 220–226 (2012).
  21. E. S. Knudsen, S. P. Angus, Regulation of DNA replication by the retinoblastoma tumor suppressor protein, in *Rb and Tumorigenesis. Molecular Biology Intelligence Unit* (Springer, 2006) pp. 20–36.
  22. A. K. Witkiewicz, S. Chung, R. Brough, P. Vail, J. Franco, C. J. Lord, E. S. Knudsen, Targeting the vulnerability of RB tumor suppressor loss in triple-negative breast cancer. *Cell Rep.* **22**, 1185–1199 (2018).
  23. T. Wilhelm, M. Said, V. Naim, DNA replication stress and chromosomal instability: Dangerous liaisons. *Genes* **11**, 642 (2020).
  24. Y. H. Park, S.-A. Im, K. Park, J. Wen, A. Min, V. Bonato, S. Park, S. Ram, D.-W. Lee, J.-Y. Kim, K.-H. Lee, W.-C. Lee, J. Lee, H. Kim, W.-W. Lee, Y.-L. Choi, S. Weinrich, H. S. Ryu, W.-Y. Park, Z. Kan, Prospective longitudinal multi-omics study of palbociclib resistance in hormone receptor+/HER2- metastatic breast cancer. *J. Clin. Oncol.* **39**, 1013 (2021).
  25. N. M. Kettner, S. Vijayaraghavan, M. G. Durak, T. Bui, M. Kohansal, M. J. Ha, B. Liu, X. Rao, J. Wang, M. Yi, J. P. W. Carey, X. Chen, T. K. Eckols, A. S. Raghavendra, N. K. Ibrahim, M. S. Karuturi, S. S. Watowich, A. Sahin, D. J. Tweardy, K. K. Hunt, D. Tripathy, K. Keyomarsi, Combined inhibition of STAT3 and DNA repair in palbociclib-resistant ER-positive breast cancer. *Clin. Cancer Res.* **25**, 3996–4013 (2019).
  26. C. H. Coschi, C. A. Ishak, D. Gallo, A. Marshall, S. Talluri, Haploinsufficiency of an RB-E2F1-Condensin II complex leads to aberrant replication and aneuploidy. *Cancer Discov.* **4**, 840–853 (2014).
  27. X. Gong, J. Du, S. H. Parsons, F. F. Merzoug, Y. Webster, P. W. Iversen, L.-C. Chio, R. D. Van Horn, X. Lin, W. Blosser, B. Han, S. Jin, S. Yao, H. Bian, C. Ficklin, L. Fan, A. Kapoor, S. Antonysamy, A. M. M. Nulty, K. Froning, D. Manglicmot, A. Pustilnik, K. Weichert, S. R. Wasserman, M. Dowless, C. Marugán, C. Baquero, M. J. Lallena, S. W. Eastman, Y.-H. Hui, M. Z. Dieter, T. Doman, S. Chu, H.-R. Qian, X. S. Ye, D. A. Barda, G. D. Plowman, C. Reinhard, R. M. Campbell, J. R. Henry, S. G. Buchanan, Aurora A kinase inhibition is synthetic lethal with loss of the RB1 tumor suppressor gene. *Cancer Discov.* **9**, 248–263 (2019).
  28. M. G. Oser, R. Fonseca, A. A. Chakraborty, R. Brough, A. Spektor, R. B. Jennings, A. Flaifel, J. S. Novak, A. Gulati, E. Buss, S. T. Younger, S. K. McBrayer, G. S. Cowley, D. M. Bonal, Q.-D. Nguyen, L. Brulle-Soumare, P. Taylor, S. Cairo, C. J. Ryan, E. J. Pease, K. Maratea, J. Travers, D. E. Root, S. Signoretti, D. Pellman, S. Ashton, C. J. Lord, S. T. Barry, W. G. Kaelin Jr., Cells lacking the RB1 tumor suppressor gene are hyperdependent on aurora B kinase for survival. *Cancer Discov.* **9**, 230–247 (2019).
  29. A. E. Marshall, M. V. Roes, D. T. Passos, M. C. DeWeerd, A. C. Chaikovskiy, J. Sage, C. J. Howlett, F. A. Dick, RB1 deletion in retinoblastoma protein pathway-disrupted cells results in DNA damage and cancer progression. *Mol. Cell. Biol.* **39**, (2019).
  30. D. Gallo, J. T. F. Young, J. Fourtounis, G. Martino, A. Álvarez-Quilón, C. Bernier, N. M. Duffy, R. Papp, A. Roulston, R. Stocco, J. Szychowski, A. Veloso, H. Alam, P. S. Baruah, A. B. Fortin, J. Bowlan, N. Chaudhary, J. Desjardins, E. Dietrich, S. Fournier, C. Fugère-Desjardins, T. G. de Rugy, M.-E. Leclaire, B. Liu, V. Bhaskaran, Y. Mamane, H. Melo, O. Nicolas, A. Singhanía, R. K. Szilard, J. Tkáč, S. Y. Yin, S. J. Morris, M. Zinda, C. G. Marshall, D. Durocher, CCNE1 amplification is synthetic lethal with PKMYT1 kinase inhibition. *Nature* **604**, 749–756 (2022).
  31. L. Crozier, R. Foy, B. L. Mouery, R. H. Whitaker, A. Corno, C. Spanos, T. Ly, J. Gowen Cook, A. T. Saurin, CDK4/6 inhibitors induce replication stress to cause long-term cell cycle withdrawal. *EMBO J.*, e108599 (2022).
  32. M. Fenech, M. Kirsch-Volders, A. T. Natarajan, J. Surrallés, J. W. Crott, J. Parry, H. Norppa, D. A. Eastmond, J. D. Tucker, P. Thomas, Molecular mechanisms of micronucleus, nucleoplasmic bridge and nuclear bud formation in mammalian and human cells. *Mutagenesis* **26**, 125–132 (2011).
  33. J. M. Mason, X. Wei, G. C. Fletcher, R. Kiarash, R. Brokx, R. Hodgson, I. Beletskaya, M. R. Bray, T. W. Mak, Functional characterization of CFI-402257, a potent and selective Mps1/TTK kinase inhibitor, for the treatment of cancer. *Proc. Natl. Acad. Sci. U.S.A.* **114**, 3127–3132 (2017).
  34. A. L. Manning, N. J. Dyson, pRB, a tumor suppressor with a stabilizing presence. *Trends Cell Biol.* **21**, 433–441 (2011).
  35. R. Colombo, M. Caldarelli, M. Mennecozzi, M. L. Giorgini, F. Sola, P. Cappella, C. Perra, S. R. Depaolini, L. Rusconi, U. Cucchi, N. Avanzi, J. A. Bertrand, R. T. Bossi, E. Pesenti, A. Galvani, A. Isacchi, F. Colotta, D. Donati, J. Moll, Targeting the mitotic checkpoint for cancer therapy with NMS-P715, an inhibitor of MPS1 kinase. *Cancer Res.* **70**, 10255–10264 (2010).
  36. K. L. Thu, J. Silvester, M. J. Elliott, W. Ba-Alawi, M. H. Duncan, A. C. Elia, A. S. Mer, P. Smirnov, Z. Safikhani, B. Haibe-Kains, T. W. Mak, D. W. Cescon, Disruption of the anaphase-promoting complex confers resistance to TTK inhibitors in triple-negative breast cancer. *Proc. Natl. Acad. Sci. U.S.A.* **115**, E1570–E1577 (2018).
  37. T. Eguchi, T. Takaki, H. Itadani, H. Kotani, RB silencing compromises the DNA damage-induced G<sub>2</sub>-M checkpoint and causes deregulated expression of the ECT2 oncogene. *Oncogene* **26**, 509–520 (2007).
  38. R. Vernell, K. Helin, H. Müller, Identification of target genes of the p16INK4A-pRB-E2F pathway. *J. Biol. Chem.* **278**, 46124–46137 (2003).
  39. E. S. Knudsen, R. Nambiar, S. R. Rosario, D. J. Smiraglia, D. W. Goodrich, A. K. Witkiewicz, Pan-cancer molecular analysis of the RB tumor suppressor pathway. *Commun. Biol.* **3**, 158 (2020).
  40. S. M. Harding, J. L. Benci, J. Irianto, D. E. Discher, A. J. Minn, R. A. Greenberg, Mitotic progression following DNA damage enables pattern recognition within micronuclei. *Nature* **548**, 466–470 (2017).
  41. S. M. Tolaney, A. M. Wardley, S. Zambelli, J. F. Hilton, T. A. Troso-Sandoval, F. Ricci, S.-A. Im, S.-B. Kim, S. R. Johnston, A. Chan, S. Goel, K. Catron, S. C. Chapman, G. L. Price, Z. Yang, M. C. Gainford, F. André, Abemaciclib plus trastuzumab with or without fulvestrant versus trastuzumab plus standard-of-care chemotherapy in women with hormone receptor-positive, HER2-positive advanced breast cancer (monarchER): A randomised, open-label, phase 2 trial. *Lancet Oncol.* **21**, 763–775 (2020).
  42. T. Dhir, C. W. Schultz, A. Jain, S. Z. Brown, A. Haber, A. Goetz, C. Xi, G. H. Su, L. Xu, J. Posey 3rd, W. Jiang, C. J. Yeo, T. Golan, M. J. Pishvaian, J. R. Brody, Abemaciclib is effective against pancreatic cancer cells and synergizes with HuR and YAP1 inhibition. *Mol. Cancer Res.* **17**, 2029–2041 (2019).
  43. M. Garutti, G. Targato, S. Buriolla, L. Palmero, A. M. Minisini, F. Puglisi, CDK4/6 inhibitors in melanoma: A comprehensive review. *Cells* **10**, 1334 (2021).
  44. B. A. Willobe, A. A. Gaidarski, A. R. Dosch, J. A. Castellanos, X. Dai, S. Mehra, F. Messaggio, S. Srinivasan, M. N. VanSaun, N. S. Nagathihalli, N. B. Merchant, Combined blockade of MEK and CDK4/6 pathways induces senescence to improve survival in pancreatic ductal adenocarcinoma. *Mol. Cancer Ther.* **20**, 1246–1256 (2021).

45. C. Dominguez-Brauer, K. L. Thu, J. M. Mason, H. Blaser, M. R. Bray, T. W. Mak, Targeting mitosis in cancer: Emerging strategies. *Mol. Cell* **60**, 524–536 (2015).
46. S. T. Pachis, G. J. P. L. Kops, Leader of the SAC: Molecular mechanisms of Mps1/TTK regulation in mitosis. *Open Biol.* **8**, 180109 (2018).
47. S. Simon Serrano, W. Sime, Y. Abassi, R. Daams, R. Massoumi, M. Jemaà, Inhibition of mitotic kinase Mps1 promotes cell death in neuroblastoma. *Sci. Rep.* **10**, 11997 (2020).
48. M. Choi, Y. H. Min, J. Pyo, C.-W. Lee, C.-Y. Jang, J.-E. Kim, Tc Mps1 12, a novel Mps1 inhibitor, suppresses the growth of hepatocellular carcinoma cells via the accumulation of chromosomal instability. *Br. J. Pharmacol.* **174**, 1810–1825 (2017).
49. A. Faisal, G. W. Y. Mak, M. D. Gurden, C. P. R. Xavier, S. J. Anderhub, P. Innocenti, I. M. Westwood, S. Naud, A. Hayes, G. Box, M. R. Valenti, A. K. De H. Brandon, L. O'Fee, J. Schmitt, H. L. Woodward, R. Burke, R. L. M. van Montfort, J. Blagg, F. I. Raynaud, S. A. Eccles, S. Hoelder, S. Linardopoulos, Characterisation of CCT271850, a selective, oral and potent MPS1 inhibitor, used to directly measure in vivo MPS1 inhibition vs therapeutic efficacy. *Br. J. Cancer* **116**, 1166–1176 (2017).
50. I. Alimova, J. Ng, P. Harris, D. Birks, A. Donson, M. D. Taylor, N. K. Foreman, S. Venkataraman, R. Vibhakar, MPS1 kinase as a potential therapeutic target in medulloblastoma. *Oncol. Rep.* **36**, 2633–2640 (2016).
51. K. D. Tardif, A. Rogers, J. Cassiano, B. L. Roth, D. M. Cimbara, R. McKinnon, A. Peterson, T. B. Douce, R. Robinson, I. Dorweiler, T. Davis, M. A. Hess, K. Ostanin, D. I. Papac, V. Baichwal, I. McAlexander, J. A. Willardsen, M. Saunders, H. Christophe, D. V. Kumar, D. A. Wettstein, R. O. Carlson, B. L. Williams, Characterization of the cellular and antitumor effects of MPI-0479605, a small-molecule inhibitor of the mitotic kinase Mps1. *Mol. Cancer Ther.* **10**, 2267–2275 (2011).
52. Y. Cohen-Sharir, J. M. McFarland, M. Abdusamad, C. Marquis, S. V. Bernhard, M. Kazachkova, H. Tang, M. R. Ippolito, K. Laue, J. Zerbib, H. L. H. Malaby, A. Jones, L.-M. Stautmeister, I. Bockaj, R. Wardenaar, N. Lyons, A. Nagaraja, A. J. Bass, D. C. J. Spierings, F. Fojier, R. Beroukhim, S. Santaguida, T. R. Golub, J. Stumpff, Z. Storchová, U. Ben-David, Aneuploidy renders cancer cells vulnerable to mitotic checkpoint inhibition. *Nature* **590**, 486–491 (2021).
53. S. J. Anderhub, G. W.-Y. Mak, M. D. Gurden, A. Faisal, K. Drosopoulos, K. Walsh, H. L. Woodward, P. Innocenti, I. M. Westwood, S. Naud, A. Hayes, E. Theofani, S. Filosto, H. Saville, R. Burke, R. L. M. van Montfort, F. I. Raynaud, J. Blagg, S. Hoelder, S. A. Eccles, S. Linardopoulos, High proliferation rate and a compromised spindle assembly checkpoint confers sensitivity to the MPS1 inhibitor BOS172722 in triple-negative breast cancers. *Mol. Cancer Ther.* **18**, 1696–1707 (2019).
54. M. O. Freitas, J. Gartner, A. Rangel-Pozzo, S. Mai, Genomic instability in circulating tumor cells. *Cancers (Basel)* **12**, 3001 (2020).
55. M. Jemaà, L. Galluzzi, O. Kepp, A. Boilève, D. Lissa, L. Senovilla, F. Harper, G. Pierron, F. Berardinelli, A. Antocchia, M. Castedo, I. Vitale, G. Kroemer, Preferential killing of p53-deficient cancer cells by reversion. *Cell Cycle* **11**, 2149–2158 (2012).
56. M. Jemaà, L. Galluzzi, O. Kepp, L. Senovilla, M. Brands, U. Boerner, M. Koppitz, P. Lienau, S. Precht, V. Schulze, G. Siemester, A. M. Wengner, D. Mumberg, K. Ziegelbauer, A. Abrieu, M. Castedo, I. Vitale, G. Kroemer, Characterization of novel MPS1 inhibitors with preclinical anticancer activity. *Clin. Death Differ.* **20**, 1532–1545 (2013).
57. S. Goel, M. J. DeCristo, A. C. Watt, H. BrinJones, J. Sceneay, B. B. Li, N. Khan, J. M. Ubellacker, S. Xie, O. Metzger-Filho, J. Hoog, M. J. Ellis, C. X. Ma, S. Ramm, I. E. Krop, E. P. Winer, T. M. Roberts, H.-J. Kim, S. S. McAllister, J. J. Zhao, CDK4/6 inhibition triggers anti-tumour immunity. *Nature* **548**, 471–475 (2017).
58. C. De Angelis, X. Fu, M. L. Cataldo, A. Nardone, R. Pereira, J. Veeraraghavan, S. Nanda, L. Qin, V. Sethunath, T. Wang, S. G. Hilsenbeck, M. Benelli, I. Migliaccio, C. Guarducci, L. Malorni, L. M. Litchfield, J. Liu, J. Donaldson, P. Selenica, D. N. Brown, B. Weigelt, J. S. Reis-Filho, B. H. Park, S. A. Hurvitz, D. J. Slamon, M. F. Rimawi, V. M. Jansen, R. Jeselsohn, C. K. Osborne, R. Schiff, Activation of the interferon signaling pathway is associated with resistance to CDK4/6 inhibitors and immune checkpoint activation in ER-positive breast cancer. *Clin. Cancer Res.* **27**, 4870–4882 (2021).
59. X. Wu, X. Yang, Y. Xiong, R. Li, T. Ito, T. A. Ahmed, Z. Karoulia, C. Adamopoulos, H. Wang, L. Wang, L. Xie, J. Liu, B. Ueberheide, S. A. Aaronson, X. Chen, S. G. Buchanan, W. R. Sellers, J. Jin, P. I. Poulikakos, Distinct CDK6 complexes determine tumor cell response to CDK4/6 inhibitors and degraders. *Nat. Cancer* **2**, 429–443 (2021).
60. C. L. Alves, S. Ehmsen, M. G. Terp, N. Portman, M. Tuttolomondo, O. L. Gammellaard, M. F. Hundebøl, K. Kaminska, L. E. Johansen, M. Bak, G. Honeth, A. Bosch, E. Lim, H. J. Ditzel, Co-targeting CDK4/6 and AKT with endocrine therapy prevents progression in CDK4/6 inhibitor and endocrine therapy-resistant breast cancer. *Nat. Commun.* **12**, 5112 (2021).
61. C. Michaloglou, C. Crafter, R. Siersbaek, O. Delpuech, J. O. Curwen, L. S. Carnevalli, A. D. Staniszewska, U. M. Polanska, A. Cheraghchi-Bashi, M. Lawson, I. Chernerukhin, R. McEwen, J. S. Carroll, S. C. Cosulich, Combined inhibition of mTOR and CDK4/6 is required for optimal blockade of E2F function and long-term growth inhibition in estrogen receptor-positive breast cancer. *Mol. Cancer Ther.* **17**, 908–920 (2018).
62. A. M. Safonov, C. Bandlamudi, P. Selenica, A. Marra, E. Ferraro, D. Mandelker, D. B. Solit, M. F. Berger, L. Norton, S. N. Powell, R. Shen, M. E. Robson, S. Chandralapaty, J. S. Reis-Filho, P. Razavi, Allelic dosage of RB1 drives CDK4/6 inhibitor treatment resistance in metastatic breast cancer. *J. Clin. Orthod.* **40**, –1010 (2022).
63. J. Hilton, D. J. Renouf, D. W. Cescon, A. R. Hansen, A. R. A. Razak, L.-A. Stayner, T. Denny, G. Fletcher, T. W. Mak, M. Bray, P. L. Bedard, Abstract P1-18-17: Phase I study of cfi-402257, an oral ttk inhibitor, in patients with advanced solid tumors with breast cancer expansion cohorts. *Cancer Res.* **82**, P1–18–17 (2022).
64. D. W. Cescon, S. V. Bratman, S. M. Chan, L. L. Siu, Circulating tumor DNA and liquid biopsy in oncology. *Nat. Cancer* **1**, 276–290 (2020).
65. N. Sachs, J. de Ligt, O. Kopper, E. Gogola, G. Bounova, F. Weeber, A. V. Balgobind, K. Wind, A. Gracanin, H. Begthel, J. Korving, R. van Boxtel, A. A. Duarte, D. Lelieveld, A. van Hoek, R. F. Ernst, F. Blokzijl, I. J. Nijman, M. Hoogstraat, M. van de Ven, D. A. Egan, V. Zinzalla, J. Moll, S. F. Boj, E. E. Voest, L. Wessels, P. J. van Diest, S. Rottenberg, R. G. J. Vries, E. Cuppen, H. Clevers, A living biobank of breast cancer organoids captures disease heterogeneity. *Cell* **172**, 373–386.e10 (2018).
66. J. P. Bruce, K.-F. To, V. W. Y. Lui, G. T. Y. Chung, Y.-Y. Chan, C. M. Tsang, K. Y. Yip, B. B. Y. Ma, J. K. S. Woo, E. P. Hui, M. K. F. Mak, S.-D. Lee, C. Chow, S. Velapasamy, Y. Y. Or, P. K. Siu, S. El Ghamrasni, S. Prokopec, M. Wu, J. S. H. Kwan, Y. Liu, J. Y. K. Chan, C. A. van Hasselt, L. S. Young, C. W. Dawson, I. C. Paterson, L.-F. Yap, S.-W. Tsao, F.-F. Liu, A. T. C. Chan, T. J. Pugh, K.-W. Lo, Whole-genome profiling of nasopharyngeal carcinoma reveals viral-host co-operation in inflammatory NF- $\kappa$ B activation and immune escape. *Nat. Commun.* **12**, 4193 (2021).
67. P. Smirnov, Z. Safikhani, N. El-Hachem, D. Wang, A. She, C. Olsen, M. Freeman, H. Selby, D. M. A. Gendoo, P. Grossmann, A. H. Beck, H. J. W. L. Aerts, M. Lupien, A. Goldenberg, B. Haibe-Kains, PharmacogX: An R package for analysis of large pharmacogenomic datasets. *Bioinformatics* **32**, 1244–1246 (2016).
68. Y. Liu, R. Laufer, N. K. Patel, G. Ng, P. B. Sampson, S.-W. Li, Y. Lang, M. Feher, R. Brokx, I. Beletskaya, R. Hodgson, O. Plotnikova, D. E. Awrey, W. Qiu, N. Y. Chirgadze, J. M. Mason, X. Wei, D. C.-C. Lin, Y. Che, R. Kiarash, G. C. Fletcher, T. W. Mak, M. R. Bray, H. W. Pauls, Discovery of pyrazolo[1,5-a]pyrimidine TTK inhibitors: CFI-402257 is a potent, selective, bioavailable anticancer agent. *ACS Med. Chem. Lett.* **7**, 671–675 (2016).
69. R. Marcotte, A. Sayad, K. R. Brown, F. Sanchez-Garcia, J. Reimand, M. Haider, C. Virtanen, J. E. Bradner, G. D. Bader, G. B. Mills, D. Pe'er, J. Moffat, B. G. Neel, Functional genomic landscape of human breast cancer drivers, vulnerabilities, and resistance. *Cell* **164**, 293–309 (2016).

**Acknowledgments:** We thank the members of the D.W.C. and T.W.M. laboratories for experimental and scientific discussions, the Princess Margaret Living Biobank ([www.livingbiobank.ca](http://www.livingbiobank.ca)) for collaborating in the establishment of PDOs, and B. Neel for sharing breast cancer cell lines. **Funding:** This work was supported by SU2C Canada–Canadian Cancer Society Breast Cancer Dream Team Research Funding SU2C-AACR-DT-18-15 (to D.W.C., B.H.-K., and T.W.M.); Canadian Institutes of Health Research PJT-175317 (to D.W.C., B.H.-K., and I.S.-B.); Terry Fox Research Institute, Program Project Grant PPG-1064 (to D.W.C.); Princess Margaret Cancer Foundation (to D.W.C.); DH Gales Family Foundation (to D.W.C.); the CIHR Postdoctoral Fellowship Award (to I.S.-B.); and TransMedTech Institute and Apogee Canada Research Excellence Fund (to A.A.N.R.). **Author contributions:** Conceptualization: I.S.-B., D.W.C., and T.W.M. Methodology: I.S.-B., D.W.C., T.W.M., K.L.T., and S.E.G. Investigation: I.S.-B., K.L.T., J.S., J.C., S.E.G., J.J.C., A.C.E., G.C.F., and R.K. Formal analysis: I.S.-B., S.E.G., W.B., M.J.E., and A.C. Visualization: I.S.-B. and D.W.C. Funding acquisition: D.W.C., T.W.M., and I.S.-B. Resources: D.W.C., T.W.M., B.H.-K., M.R.B., and A.A.N.R. Project administration: D.W.C. and I.S.-B. Supervision: D.W.C. and T.W.M. Writing—original draft: I.S.-B., K.L.T., and D.W.C. Writing—review and editing: I.S.-B., S.E.G., and D.W.C. **Competing interests:** D.W.C. reports advisory services to AstraZeneca, Exact Sciences, Eisai, Gilead, GlaxoSmithKline, Inivata, Merck, Novartis, Pfizer, and Roche; reports research funding (to institution) from AstraZeneca, Gilead, GlaxoSmithKline, Inivata, Merck, Pfizer, and Roche; and is a member of a trial steering committee for AstraZeneca, Merck, and GlaxoSmithKline. D.W.C. and B.H.-K. hold a patent (US62/675,228) for methods of treating cancers characterized by a high expression level of spindle and kinetochore associated complex subunit 3 (*SKA3*) gene. G.C.F., R.K., and M.R.B. are current employees of Treadwell Therapeutics, which is developing CFI-402257. T.W.M. is a founder and equity holder in Agios and Treadwell Therapeutics, is a Scientific Advisory Board member for AstraZeneca and Tessa Therapeutics, and holds patents related to this work. A.A.N.R. reports advisory services to Pfizer and has a family member who is employed by Merck. All other authors declare no competing interests. **Data and materials availability:** All data needed to evaluate the conclusions in the paper are present in the paper and/or the Supplementary Materials. Sequencing files are available via Zenodo: 10.5281/zenodo.6760819 (cell lines) and 10.5281/zenodo.6800381 (organoids). The cell lines and organoids can be provided by the corresponding author pending scientific review and a completed material transfer agreement. Requests for these materials should be submitted to the corresponding author.

Submitted 7 April 2022

Accepted 21 July 2022

Published 7 September 2022

10.1126/sciadv.abq4293